

Extended Card Modulation - Test Methods

Master's Thesis

MA 702

Jürgen Hölzl

Institute for Electronics (IFE)
Graz University of Technology
Interim Head: Univ.-Prof. Dipl.-Ing. Dr.techn. Wolfgang Bösch



supported by Infineon Technologies Austria AG

Assessor:
Univ.-Prof. Dipl.-Ing. Dr.techn. Peter Söser
Advisor: Dipl.-Ing. Josef Gruber (Infineon)

Graz, December 2011



Never stop thinking

This Master Thesis is supported by
Infineon Technologies Austria AG
Development Center Graz
Department of Chip Card and Security System
Head: Peter Raggam

Abstract

This master thesis deals with the contactless data transfer between a chip card and a reader, which is known as *RFID system* (Radio Frequency Identification). Basically, the reader provides energy and a clock signal to the card by means of inductive coupling. The data transmission from the reader to the card is performed by means of amplitude modulation at a carrier frequency of 13.56 MHz. Vis-a-vis , the card transfers data to the terminal by varying its load and thus evoking noticeable reaction to the reader. This modulation is called *load modulation*. It has a defined period and thus generates a new frequency in the signal spectrum, which is called *subcarrier frequency*. Generally, the load modulation is done by varying the ohmic or capacitive load of the chip. This modulation method causes a change of the carrier signal's amplitude and phase due to the detuning of the resonance circuit and can be considered as a combination of amplitude and phase modulation.

The aim of this work was to create an analysis program, which more accurately analyzes the load modulation of the chip card and its impact on the reader. In addition, an attention should be given especially to the various contactless chip types of Infineon. In particular, the analysis of the load modulation refers to the standardized measurement methods for proximity smart cards. During this thesis, different measurement methods were investigated and evaluated.

Keywords: RFID, Chip Card, Load Modulation, Standardization, ISO/IEC 14443

Kurzfassung

Hauptaugenmerk dieser Masterarbeit ist die Analyse der kontaktlosen Datenübertragung einer Chipkarte zum Lesegerät, welches als *RFID System* (Radio Frequency Identification) bekannt ist. Grundsätzlich versorgt das Lesegerät die Karte mit Energie und einem Taktsignal mittels induktiver Kopplung. Typischerweise wird die Datenübertragung vom Lesegerät zur Karte über eine Amplitudenmodulation bei einer Trägerfrequenz von 13,56 MHz durchgeführt. In entgegengesetzte Richtung überträgt die Karte ihre Daten indem sie ihre Last variiert und somit eine unterschiedliche Rückwirkung auf das Lesegerät hervorruft. Diese Modulation wird als *Lastmodulation* bezeichnet und wird in der Praxis in einem Subträger übermittelt, da das Signal im Vergleich zum Trägersignal sehr klein ist. Übliche Verfahren für die Lastmodulation sind die Änderung der ohmschen bzw. der kapazitiven Last. Prinzipiell bewirkt das Modulationsverfahren eine Änderung der Amplitude und Phase des Trägersignals aufgrund der Verstimmung des Resonanzkreises in der Karte und kann als Kombination aus einer Amplituden- und Phasenmodulation betrachtet werden.

Ziel dieser Arbeit war die Erstellung eines Analyseprogramms, welches die Lastmodulation der Karte und ihre Auswirkung auf das Lesegerät genauer analysiert und qualitativ beurteilt. Des Weiteren sollte speziell ein Augenmerk auf die Analyse der verschiedenen kontaktlosen Chipkartentypen von Infineon gelegt werden. Im Speziellen bezieht sich die Analyse der Lastmodulation auf die standardisierten Messverfahren für Proximity Chipkarten. Überdies wurden diese Verfahren genauer betrachtet und evaluiert.

Stichwörter: RFID, Chip Karte, Last Modulation, Standardisierung, ISO/IEC 14443

EIDESSTATTLICHE ERKLÄRUNG

Ich erkläre an Eides statt, dass ich die vorliegende Arbeit selbstständig verfasst, andere als die angegebenen Quellen/Hilfsmittel nicht benutzt, und die den benutzten Quellen wörtlich und inhaltlich entnommenen Stellen als solche kenntlich gemacht habe.

Graz, am

.....

(Unterschrift)

STATUTORY DECLARATION

I declare that I have authored this thesis independently, that I have not used other than the declared sources / resources, and that I have explicitly marked all material which has been quoted either literally or by content from the used sources.

.....

date

.....

(signature)

Acknowledgment

It took quite a long time to find the best master thesis theme at the end of my telematic study. Like my nice fellow, with whom I now care a good friendship, I have luckily decided to do my thesis at the company Infineon Technologies Austria AG. I would like to say thank you very much for giving me the chance to work in such a professional and friendly team. I wish to express my gratitude for the excellent support to Peter Raggam, Josef Gruber, Stephan Rampetzreiter and the other CL SYS team members. Furthermore I want to thank Professor Peter Soeser for the professional support during my thesis.

Last but not least I want to explain my greatest thanks to my family, my parents Josef and Ulrike, my siblings Jörg, Robert, Christoph and Sarah, and my grandparents Johann and Hilde for the financial and human assistance.

Jürgen Hölzl

Contents

1	Introduction	1
1.1	Motivation	1
1.2	Structure of Thesis	2
2	RFID Basics	3
2.1	Components of an RFID System	3
2.1.1	RFID Transponder	4
2.1.2	RFID Reader	5
2.2	Classification of an RFID System	6
3	Physical Fundamentals of RFID Systems	7
3.1	Magnetic field strength H	7
3.2	Magnetic flux and magnetic flux density	8
3.3	Self-Inductance L	9
3.4	Mutual Inductance M	10
3.5	Inductively Coupled System	11
3.6	Resonance Circuit	13
3.7	Quality Factor	15
4	System Description	17
4.1	Proximity Coupling Device (PCD)	17
4.2	Proximity Integrated Circuit Card (PICC)	19
4.3	Transformed Transponder Impedance	23
4.4	Data Communication	26
4.4.1	Communication from PCD to PICC	28
4.4.2	Communication from PICC to PCD	30

5	Standardized Measurement Methods	38
5.1	ISO Set-up	39
5.1.1	VLMA	39
5.1.2	Test Set-up	41
5.1.3	H field calculation	46
5.2	EMVCo Set-up	50
6	LM Analysis Tool	54
6.1	Measuring and Analysis Process	54
6.1.1	General Steps	54
6.1.2	Measuring Arrangement	55
6.2	Data Analysis	57
6.2.1	Voltage Load Modulation Amplitude	57
6.2.2	Amplitude Difference	57
6.2.3	Phase Difference	58
6.2.4	Amplitude of Difference Vector	58
6.2.5	Pointer Diagram of Signal	58
6.2.6	Overshoot/Undershoot and Rise/Fall Time of Amplitude and Phase	59
6.2.7	Equivalent Circuit	60
6.2.8	EMVCo Vpp Estimation	67
6.3	Program Structure and Functions	67
6.3.1	Main GUI	68
6.3.2	Function LMAnalyze	70
6.3.3	Function importfile	71
6.3.4	Function makeFFT	71
6.3.5	Function DetectDistribution	72
6.3.6	Function DetectEMVCo	73
6.3.7	Function AnalyzeWaveform	73
6.3.8	Function Equivalent Circuit	75
6.3.9	Function EMVCo Vpp	76
7	Conclusion	77
	Bibliography	79

List of Figures

2.1	RFID-System [5]	3
2.2	Layout of a contactless smart card with antenna and transponder (adapted from [5])	4
2.3	Dual Interface RFID Reader with USB connection	5
3.1	Magnetic flux over a current-carrying conductor and coil [5]	7
3.2	Illustration of magnetic flux Φ in area A and flux density B [5]	9
3.3	Mutual Inductance M of two coils [5]	10
3.4	Two inductively coupled coils and their equivalent circuit [5]	11
3.5	Serial resonant circuit [11]	13
3.6	Parallel resonant circuit [11]	14
3.7	Bandwidth and resonance frequency of a resonant circuit	16
4.1	Equivalent circuit of a PCD	18
4.2	Basic equivalent circuit of a PICC	20
4.3	PICC equivalent circuit for calculation	21
4.4	PICC equivalent circuit with rectifier and shunt resistor	22
4.5	Shunt mechanism for voltage regulation	23
4.6	Quality factor of PICC	24
4.7	Equivalent circuit for transformed transponder impedance	25
4.8	Transformed transponder impedance as a function of the coupling factor	27
4.9	PCD antenna current as a function of the transformed transponder impedance	27
4.10	ASK with 100% modulation index, NRZ coding	29
4.11	ASK with 10% modulation index, NRZ coding	29
4.12	Modified Miller coding [11]	30
4.13	Ohmic load modulation	30
4.14	Capacitive load modulation	31

4.15	Current i_2 according to load modulation	32
4.16	Pointer diagram of the modulated states of i_2 (example)	33
4.17	Spectrum of load modulation	34
4.18	PSK modulated signal	35
4.19	Spectrum of PSK modulated signal	35
4.20	Switching point of load modulation regarding to overshoot/undershoot . .	36
4.21	Overshoot/undershoot of i_2 related to switching point	37
5.1	VLMA Measurement: Values at upper and lower sideband [2]	40
5.2	Minimum VLMA values according to ISO/IEC 14443 [7]	40
5.3	ISO-Measurement set-up [2]	42
5.4	Cross section of ISO-Tower	42
5.5	Bridge connection of ISO-tower [2]	44
5.6	Electrical equivalent circuit of the measuring bridge [2]	44
5.7	Compensation of error voltage with potentiometer	45
5.8	Frequency dependency of error vector	46
5.9	Card field geometry of calibration coil	47
5.10	Front view of the EMVCo-Tower	50
5.11	Equivalent circuit for EMVCo Set-up	51
5.12	PCD current i_1 at load modulation	53
5.13	Demodulated signal and definition of V_{pp}	53
6.1	ISO-Measuring arrangement	55
6.2	Amplitude difference of modulated current	57
6.3	Phase difference of modulated current	58
6.4	Pointer diagram of signal states	59
6.5	Waveform parameters (adapted from [1])	60
6.6	PICC equivalent circuit for calculation	61
6.7	Correction factor for i_2 without and with error compensation for different coupling factors	63
6.8	Correction factor for i_2 without and with error compensation for different sense coil values	64
6.9	Experiment: Noise vector compensation	66
6.10	Program functions and calling structure	68
6.11	Graphical User Interface	69

6.12	Detection of distribution via histogram analysis	74
6.13	Gaussian fitting algorithm for state detection	75

List of Tables

5.1	Values for ISO-Tower	43
5.2	Values for EMVCo PCD	51
5.3	Coupling factors and mutual inductances of PCD and PICC (4 coil turns, ID1)	52
5.4	Measured field strength at slots with calibration coil	52

Chapter 1: Introduction

Radio Frequency Identification (RFID) is a very fast growing market and enables the contactless identification of objects, items, animals and persons. In recent years, many new innovative applications were invented and a lot of companies are doing their research in this area. One of the most common applications is the anti-theft system in department stores, which protects articles with a small identification chip from robbery. Other common uses of RFID are access control of persons, contactless payment via credit card and labeling of articles and animals in industry and research. There are some different complex solutions for enabling the communication between transponder and reader, but they are all based on the physical fundamentals of RFID.

This master thesis deals with the contactless data transfer from a proximity card to the reader. The data transmission from the reader to the card is carried out on an amplitude modulation at a carrier frequency of 13.56 MHz. The card transfers the data to the terminal by varying its load and thus evokes a different repercussion on the reader. This modulation is called load modulation and is delivered in practice in a subcarrier, since the signal compared to the carrier signal is very small. The normal procedure for the load modulation is the change of the resistive or capacitive load. This modulation method causes a change in the amplitude and phase of the carrier due to the change of the resonance circuit in the transponder and can be considered as a combination of an amplitude and phase modulation. This procedure will be analyzed and evaluated more accurately in this thesis.

1.1 Motivation

The data transfer of a contactless proximity smart card is a special challenge, because the card has no active supply voltage by means of a battery and it has to gain its energy from the electromagnetic field. The modulation from the card to the reader can not generally be realized as the modulation from the reader to the card, because of the small

geometric dimensions of the card and the limited energy. This data transfer happens namely on a passive way by changing the load in the card to influence the seen load by the reader (load modulation). This system of interaction is very complex and will be considered in a more accurate analysis. The specification in ISO/IEC 14443 (the International Organization for Standardization) describes the structure, communication and modulation of the RFID system and its standards to be met. According to the standard, load modulation is measured by the energy level at the two sidebands in the frequency spectrum. Necessarily, this type of analysis does not give a guaranty for a clean signal which can be correctly interpreted by the reader. Therefore, an investigation is important to achieve a better knowledge about this modulation technique and on the other hand to improve the next generations of chip cards.

1.2 Structure of Thesis

First of all, this master's thesis explains the RFID basics in chapter 2. They include the core components of an RFID system and their communication principle. Furthermore, the general classification of RFID is shown, which is divided into its operating frequency and operating range.

Chapter 3 focuses on the description of the physical fundamentals of an RFID system. That means, that the physical principles are clarified with meaningful images and mathematical formulas, which are required for the general understanding of RFID systems.

The next chapter 4 describes the RFID core components in their electrical form. It demonstrates the electrical equivalent circuit of the components and preoccupies with the mathematical description of the electrical circuits. Finally, the chapter concludes with the consideration of the data communication between the components.

The standardized measurement methods for proximity chip cards are sententiously depicted in chapter 5. Additionally, the new perceptions of the measurement systems and the measured values for the test set-ups are included.

The focus of chapter 6 lies on the self constructed load modulation analysis tool. Indeed, particularly the software structure, functionality and usage is pointed out.

Last but not least, the conclusion of the master's thesis is shown in chapter 7.

Chapter 2: RFID Basics

2.1 Components of an RFID System

Core components of an RFID system are one reader and at least one transponder. Firstly, the reader has to achieve an electromagnetic field for a defined area, which is referred to as the operating volume. Secondly, it has to manage the data communication with the transponder. The transponder represents an electronically data carrier and receives the power from the electromagnetic field of the reader, which is needed for the processor supply if no battery is available. Depending on the application these components have a different complexity. Data communication is possible in both directions and can be done with several modulation techniques and data rates. Most applications are based on the ISO/IEC standard to accomplish an international standard. The reader can be seen as the master and the transponder as the slave in the communication process. In simple applications the reader gets the identification code from the transponder which is stored on the data carrier.

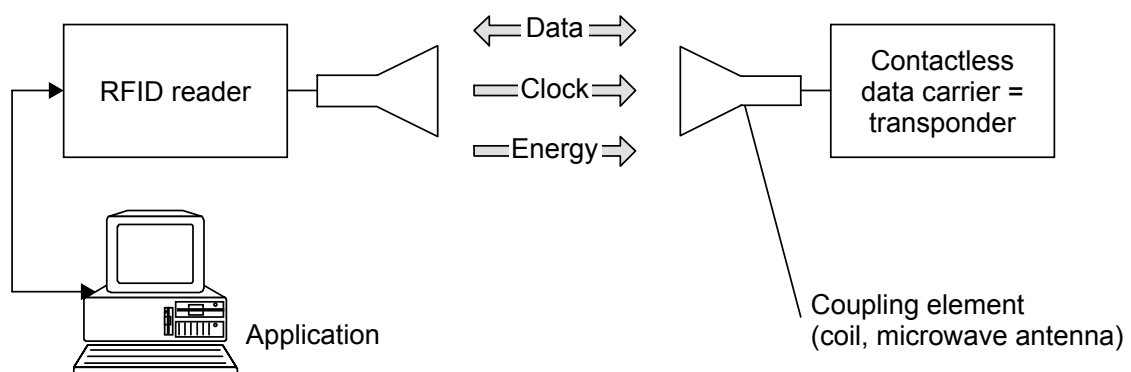


Figure 2.1: RFID-System [5]

2.1.1 RFID Transponder

Depending on the application, there exists a variety of transponders with different size, format, operating frequency, operating range, security requirements and memory capacity. Generally we separate transponders into two classes, the active transponder and the passive transponder. Active transponders have got a battery to supply their microchips and to modulate their signals for data communication. Passive transponders have to gain their energy from the electromagnetic alternating field of the reader via electrical or magnetic coupling. On the one hand active transponders have got a larger working range but on the other hand they are bigger and more expensive than the passive ones. This master thesis deals with contactless smart cards which are inductively coupled and consists of an antenna and a transponder module as shown in figure 2.2. Smart cards in an ID-1 design are very common and nearly everybody has it in his money purse. Examples are telephone cards, credit cards, driving license cards and medical cards. Because of this the following chapters focus on this type of RFID application. Contactless smart cards equipped with a microchip typically work up to a distance of 0.1 m to the reader (proximity coupling). The basic reason is that a chip card with a microchip has a higher power requirement than a simple memory card. Secondly, in payment applications it is useful to protect the owner of the card from financial fraud.

Dual-Interface-cards can be used contactless and contact-based for data communication. The ISO/IEC 14443 standard specifies the application layer and is compatible with the ISO/IEC 7816 standard for contactless chip cards. [12]

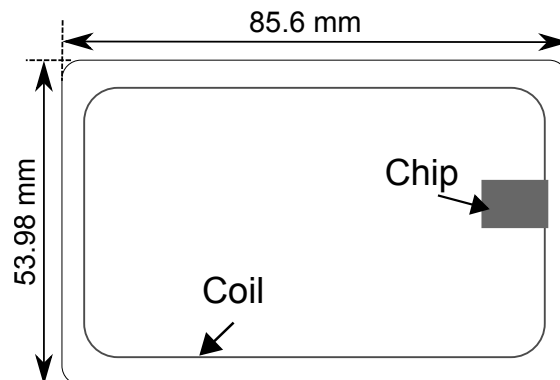


Figure 2.2: Layout of a contactless smart card with antenna and transponder (adapted from [5])

2.1.2 RFID Reader

Many useful RFID applications are common nowadays and therefore a lot of different types of readers are available. Readers are separated in a similar way as the transponders. First of all, a main attribute is the operating frequency. Secondly, readers are distinguished between their coupling mechanism. Thirdly, they have a different operating range, which depends on the coupling mechanism.

Readers are the base station of the RFID system and are available in many types. Basically, it consists of a control interface, a radio unit and a coupling device. Typical communication interfaces to a reader are RS-232, USB and Ethernet. As mentioned before, a main task of a reader is the energy supply for the transponders. Inductive coupling is the most common technology, which is based on the transformer principle. Other factors to be taken into account are anti-collision management, which handles the communication with more than one transponder in the operating range, authentication and data encryption to prevent misuse.

Figure 2.3 shows a dual interface reader, which allows the user to insert the smart card in the slot (contact based) or to communicate contact less by taking the smart card in the operating field. An USB interface allows the communication between a computer and the reader. This reader is typically used for desktop computers at home, for example for digital signing with citizen cards.



Figure 2.3: Dual Interface RFID Reader with USB connection

2.2 Classification of an RFID System

Depending on the application, there are a variety of different RFID systems available, which differ in their operating frequency, physical coupling mechanism and operating range.

RFID Systems are divided into following frequency ranges:

- Low Frequency (LF): 30 to 300 kHz
- High Frequency (HF): 3 to 30 MHz
- Ultra High Frequency (UHF): 0.3 to 3 GHz
- Super High Frequency (SHF): 3 to 30 GHz

Following operating ranges are defined:

- Close coupling: 0 to 1 cm
- Proximity coupling: 0 to 0.1 m
- Vicinity coupling: 0 to 1 m
- Long range coupling: more than 1 m

Remote coupling is the principle term for proximity and vicinity coupling. Nearly every remote coupled RFID System uses inductive coupling for data and energy transmission. One of the most common frequency range is HF, especially with a carrier frequency of 13.56 MHz, which is the focus in this document. [12]

Chapter 3: Physical Fundamentals of RFID Systems

This chapter gives a short introduction into the basic physical principles of an inductive coupled RFID system. It will be shown, how it is possible to transfer energy and data using a magnetic field between a reader and a transponder.

3.1 Magnetic field strength H

The magnetic field strength is a vector field which is created by a moving charge in wires. A common example is a current which is flowing through a wire, shown in figure 3.1. The magnetic field strength H stands for the magnitude of the magnetic field and is depended on the material properties of space [5].

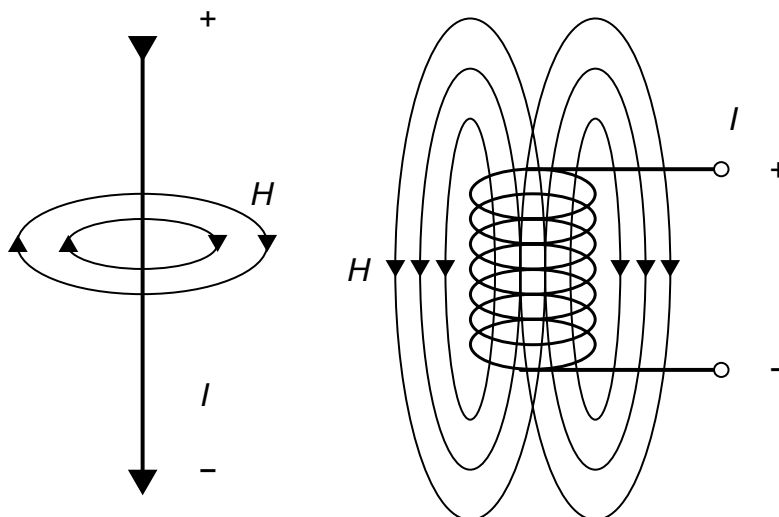


Figure 3.1: Magnetic flux over a current-carrying conductor and coil [5]

Generally, we can say that:

“the contour integral of magnetic field strength along a closed curve is equal to the sum of the current strengths of the currents within it“[9]

Quote expressed as formula:

$$\sum I = \oint \vec{H} \cdot \vec{d} s \quad (3.1.1)$$

The right side of figure 3.1 shows a current carrying cylindrical coil which is used in inductively coupled RFID systems. As you can see, there are more than one coil turns used for generating the magnetic field strength H with an alternating current I (AC). The resulting field strength can be calculated with formula 3.1.2 for a specified measuring point. R stands for the radius of N coil turns and x for the distance to the middle point of the coil.

According to formula 3.1.2 there exists an optimal antenna radius R for every read range, because the field strength H has a maximum at a certain point x for a specific radius. Increasing the radius R increases the optimal distance x too, but decreases the field strength H for very small x .

$$H = \frac{I \cdot N \cdot R^2}{2 \cdot \sqrt{(R^2 + x^2)^3}} \quad (3.1.2)$$

3.2 Magnetic flux and magnetic flux density

The magnetic flux Φ represents the amount of magnetic flux lines in a specified area A , generated by a cylindrical coil.

Formula 3.2.1 and illustration 3.2 show the relation between the magnetic flux Φ , flux density B and area A .

$$\Phi = B \cdot A \quad (3.2.1)$$

The magnetic flux density B is proportional to the magnetic field strength H , the magnetic field constant μ_0 and the relative permeability μ_r .

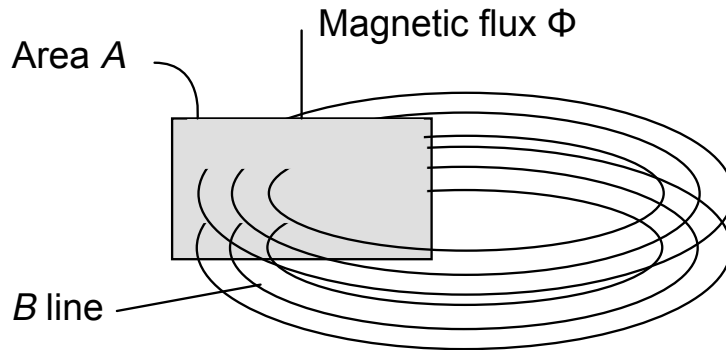


Figure 3.2: Illustration of magnetic flux Φ in area A and flux density B [5]

$$B = \mu_0 \cdot \mu_r \cdot H \quad (3.2.2)$$

$$\mu_0 = 4 \cdot 10^{-6} \cdot Vs/Am \quad (3.2.3)$$

$$\mu_r = 1 + 0.4 \cdot 10^{-6} \dots \text{ in air} \quad (3.2.4)$$

3.3 Self-Inductance L

A magnetic field is generated by an electric alternating current which is passing through a conductor. This effect can be maximized by forming one or N loops with it. The total flux is the sum of the magnetic fluxes, which are generated by the conductor loops. Generally, every conductor loop spans nearly the same area with its winding, as assumed in formula 3.3.1. The inductance L is defined as the total flux divided by the current passing through the conductor loops (formula 3.3.2). According to the *induction law*, a voltage u_i is induced by a loop which is located in an alternating magnetic flux, generated by the current i (formula 3.3.3). The differential equation in formula 3.3.4 is a general form, where the inductance represents a passive device and its voltage drop is dependent on the inductance L and the current change in time.

Under the condition of a small conductor diameter related to its spanned loop diameter, it is possible to describe the inductance L via its loop radius R , diameter d of the conductor, number of windings N and the magnetic field constant μ_0 , as shown in formula 3.3.5.

$$\psi = \sum \Phi_N = N \cdot \Phi = N \cdot \mu \cdot H \cdot A \quad (3.3.1)$$

$$L = \frac{\psi}{I} = \frac{N \cdot \Phi}{I} = \frac{N \cdot \mu \cdot H \cdot A}{I} \quad (3.3.2)$$

$$u_i = -N \cdot \frac{d\Phi}{dt} \quad (3.3.3)$$

$$u = L \cdot \frac{di}{dt} \quad (3.3.4)$$

$$L = N^2 \cdot \mu_0 \cdot R \cdot \ln\left(\frac{2R}{d}\right) \quad (3.3.5)$$

3.4 Mutual Inductance M

mutual inductance M describes the relationship between two conductor loops in a magnetic field (illustrated in figure 3.3). As mentioned before, one conductor loop has to create this magnetic flux with an alternating current through its wire and dependent on the position and the geometry of the two coils, a part of the magnetic flux flows through the second coil. This part is called coupling flux Ψ_{21} .

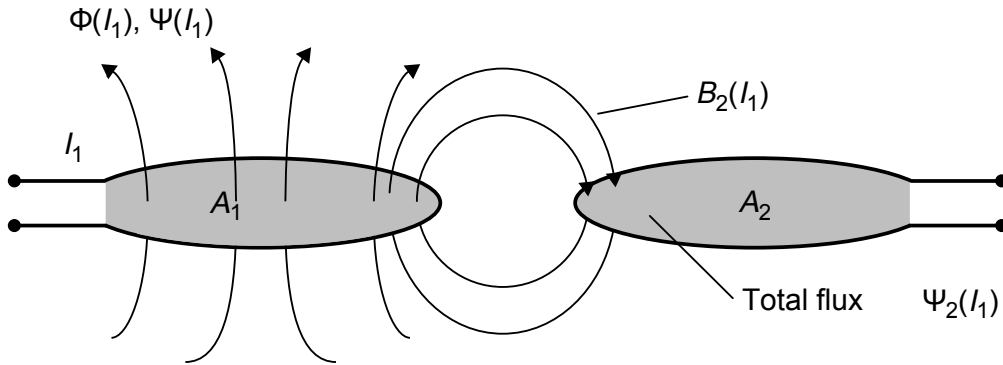


Figure 3.3: Mutual Inductance M of two coils [5]

Formula 3.4.1 shows that the mutual inductance is defined as the coupling flux Ψ_{21} divided by the current I_1 passing through the first conductor loop.

$$M_{21} = \frac{\Psi_{21}}{I_1} = \oint_{A_2} \frac{B_2(I_1)}{I_1} \cdot dA_2 \quad (3.4.1)$$

Vis-a-vis to M_{21} exists the mutual inductance M_{12} , if a current I_2 flows through the second conductor coil.

A qualitative description of an inductively coupled system of two coils gives the coupling factor k . It describes the coupled system with a factor between zero and one without any geometrical dependency of the coils. Formula 3.4.2 defines the coupling factor as the mutual inductance M divided by the square root of the product of the inductance values. If the value of the coupling factor is zero, there does not exist any coupling between the two coils. According to this, a coupling factor of one describes a perfectly coupled system, where the total magnetic flux passes through both coils.

$$k = \frac{M}{\sqrt{L_1 \cdot L_2}} \dots \text{for } 0 \leq k \leq 1 \quad (3.4.2)$$

3.5 Inductively Coupled System

Figure 3.4 shows a inductively coupled system of two coils and their electrical equivalent circuit.

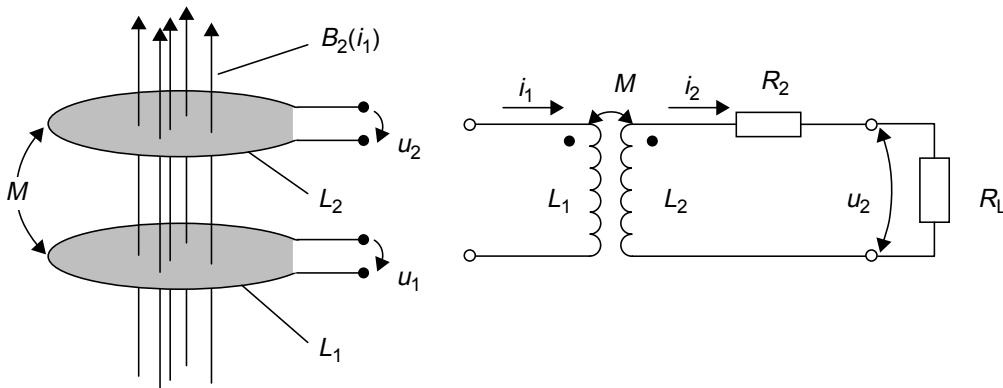


Figure 3.4: Two inductively coupled coils and their equivalent circuit [5]

The inductance L_1 is the active part of the coupled system, which is driven by the

alternating current I_1 and generates a time-depended magnetic flux. According to the inductance law, a voltage will be induced at L_1 and L_2 , which is a combination of mutual induction and self induction.

Firstly, the self induction generates a voltage in the circuit due to the alternating current di/dt . Secondly, a voltage u_2 is induced in the second circuit because of the alternating magnetic flux and the coupling of the coils (mutual inductance).

Formula 3.5.1 describes the voltage u_2 which is induced in the second circuit, where R_2 represents the internal resistance of L_2 . The first term of the formula is the voltage of the mutual inductance. The second term stands for the self induction, which is caused by the current i_2 in the second circuit. Its value is depended on the load resistor R_L (u_2/R_L). The third term describes the voltage drop at the internal resistance R_2 of the inductance L_2 , which is a function of material and layout of the coil.

$$u_2 = M \cdot \frac{di_1}{dt} - L_2 \cdot \frac{di_2}{dt} - i_2 \cdot R_2 \quad (3.5.1)$$

In somewhat simplified terms, formula 3.5.1 can be written as formula 3.5.2 when the system is driven by sinusoidal alternating currents, which is very common in praxis.

$$\underline{u}_2 = jwM \cdot \underline{i}_1 - jwL_2 \cdot \underline{i}_2 - \underline{i}_2 \cdot R_2 \quad (3.5.2)$$

Due to mutual inductance vice versa, u_1 is reduced by the second term in formula 3.5.3. This effect is very important for RFID systems because it is used for modulation by the PICC (Proximity Integrated Circuit Card) by changing the current i_2 in time. Therefore, the voltage u_1 in the PCD (Proximity Coupling Device) is influenced in time too.

$$u_1 = L_1 \cdot \frac{di_1}{dt} - M \cdot \frac{di_2}{dt} \quad (3.5.3)$$

$$\underline{u}_1 = jwL_1 \cdot \underline{i}_1 - jwM \cdot \underline{i}_2 \quad (3.5.4)$$

$$w = 2\pi f \quad (3.5.5)$$

3.6 Resonance Circuit

Principally, nearly all proximity cards are passive devices and have to gain their energy from the magnetic field of the reader. For energy maximization in the Proximity Integrated Circuit Card (PICC) the circuit has to be adapted to the resonance frequency of the reader. This is done with a resonance circuit in the Proximity Coupling Device (PCD) and in the PICC. The resonance frequency of the reader is adjusted to 13.56 MHz and the resonance frequency of the PICC is typically tuned between 12 MHz and 19 MHz. If the PICC resonance frequency is equal to the resonance frequency of the reader, the energy transfer is maximal. In practice, the PICC is tuned to higher frequencies because of some critical effects that will be discussed later.

Figure 3.5 represents a serial resonant circuit and formula 3.6.1 defines the impedance of the circuit. The resonance frequency f_{res} according to phase resonance condition can be calculated through the angular frequency ω . The imaginary part of Z must be zero for phase resonance. The combination of formula 3.5.5 with formula 3.6.2 leads to the result for the resonance frequency in formula 3.6.3, which is known as the Thomson equation. Secondly, the resonance frequency can be evaluated by measuring the absolute value, which is maximal at resonance frequency. Thirdly, the resonance frequency can be measured by measuring the maximal real part value of the impedance, which indicates the resonance frequency. This way is typical in practice, when it is measured by a network analyzer (illustrated in figure 3.7).

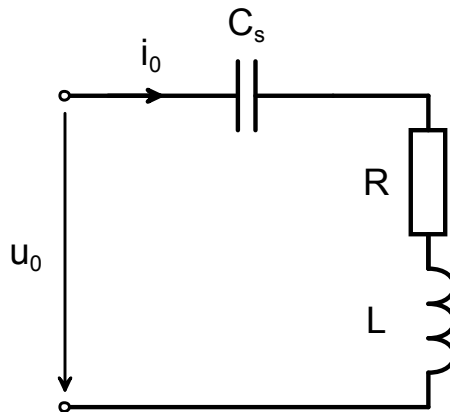


Figure 3.5: Serial resonant circuit [11]

$$\underline{Z}_{serial} = j\omega L + R + \frac{1}{j\omega C} = R + j \cdot \left(\omega L - \frac{1}{\omega C} \right) \quad (3.6.1)$$

$$\Im \{ \underline{Z}_{serial} \} \stackrel{!}{=} 0 \Rightarrow \omega_{res,serial} = \frac{1}{\sqrt{L \cdot C}} \quad (3.6.2)$$

$$f_{res,serial} = \frac{1}{2\pi \cdot \sqrt{L \cdot C}} \quad (3.6.3)$$

The parallel resonance circuit in figure 3.6 is the typical resonance circuit in a PICC. The resistor R is a result of the losses from the inductance L and is often hard to evaluate because it is frequency depended and very small. The serial resistor can be mathematically converted to a parallel resistor which leads to the common version of a parallel resonance circuit.

Unlike to the resonance frequency of the serial resonance circuit, the serial resistor R influences the resonance frequency of the parallel resonance circuit (formula 3.6.4). Setting the imaginary part of $Z_{parallel}$ to zero, leads to the resonance frequency for the parallel resonance circuit (formula 3.6.5).

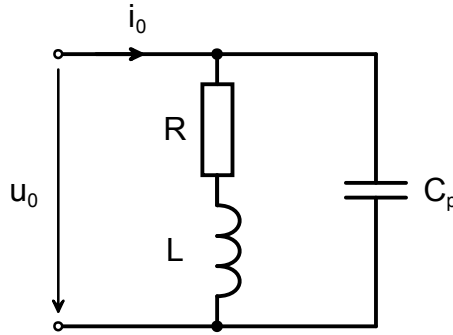


Figure 3.6: Parallel resonant circuit [11]

$$\underline{Z}_{parallel} = \frac{(j\omega L + R) \cdot \frac{1}{j\omega C_p}}{j\omega L + R + \frac{1}{j\omega C_p}} = \frac{j\omega L + R}{Rj\omega C_p - \omega^2 LC_p + 1} \quad (3.6.4)$$

$$f_{res,parallel} = \frac{1}{2\pi} \cdot \sqrt{\frac{1}{L \cdot C_p} - \frac{R^2}{L^2}} \quad (3.6.5)$$

3.7 Quality Factor

Principally, the quality factor Q is dimensionless and describes how much a oscillation is damped by the losses in a resonance circuit. The damping factor d is reciprocal to Q (formula 3.7.1). Generally, the quality factor is defined as the quotient of the stored energy in the resonance circuit to the supplied energy by the generator. Voltage and current step-up are measured in the resonance circuit to evaluate Q . The quality factor for a serial resonance circuit is defined in formula 3.7.2 and for the parallel resonance circuit in formula 3.7.3.

$$d = \frac{1}{Q} \quad (3.7.1)$$

$$Q_{serial} = \frac{w \cdot L}{R} = \frac{1}{R} \cdot \sqrt{\frac{L}{C}} \quad (3.7.2)$$

$$Q_{parallel} = R_p \cdot \sqrt{\frac{L}{C}} \quad (3.7.3)$$

As shown in figure 3.7, the resonance frequency can be measured through the detection of the maximum peak from the real part of the resonance circuit impedance. The bandwidth B is defined as the difference between the upper half power point and the lower half power point. With regard to figure 3.7 this points are the -3 dB points in the curve related to the peak value.

The larger the bandwidth B of a resonance circuit, the lower the quality factor Q . Hence, a compromise between the bandwidth B and the quality factor Q has to be chosen for an RFID system. The energy transfer from the PCD to the PICC can be maximized by a high quality factor, but it has negative consequences to the data transfer in both directions, because the side lobes are attenuated very effectively. In view of a high bandwidth, the operating range of the RFID system would be limited. Related to figure 3.7 a high quality factor leads to a high peak at the resonance frequency f_{res} , but narrows the curve at its middle. Or, the other way round, a high bandwidth B shrinks the maximum peak, but widens the middle.

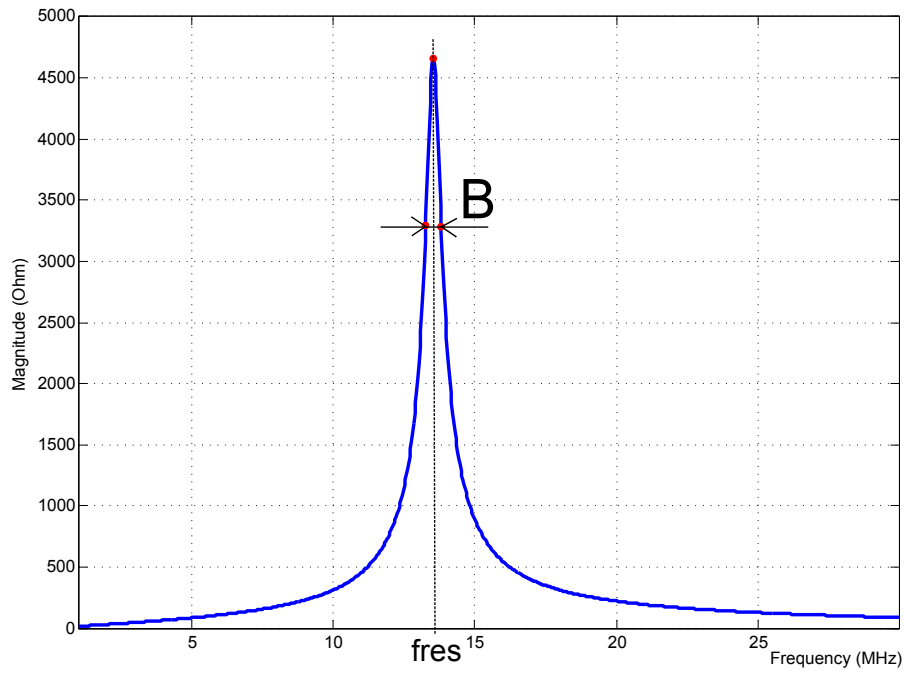


Figure 3.7: Bandwidth and resonance frequency of a resonant circuit

Formula 3.7.4 represents the discussed problem in a mathematical form.

$$Q_{res} = \frac{f_{res}}{B} \quad (3.7.4)$$

Chapter 4: System Description

This chapter describes the components of an RFID system, as explained in chapter 2, in their electrical form. The focus of the section is on the description of a proximity coupled system via its electrical equivalent circuits.

4.1 Proximity Coupling Device (PCD)

Principally, a PCD can be seen as a simple serial resonance circuit, which is driven with an alternating current at 13.56 MHz. In reality, the external supply has an internal serial resistor R_i , which's value is typically 50 Ohm. Therefore, an adaptive matching circuit for the antenna is needed to match the resonance circuit with 50 Ohm. In order to achieve this matching, a serial and parallel capacity is used (C_{mp} and C_{ms}). The circuit is matched, when the impedance of the antenna circuit has exactly 50 Ohm, which presupposes that the imaginary part is zero. This type of matching is called power adjustment and the power efficiency is 50 percent.

Under these circumstances, the equivalent circuit of a PCD changes to the circuit in figure 4.1.

As described earlier, following requirements for power adjustment have to be met:

- $\underline{Z}_{PCD} = \Re\{\underline{Z}_{PCD}\} + j \cdot \Im\{\underline{Z}_{PCD}\}$
- $\Re\{\underline{Z}_{PCD}\} \stackrel{!}{=} 50$
- $\Im\{\underline{Z}_{PCD}\} \stackrel{!}{=} 0$

Under the required conditions for the matching network, the solution for the two capacitors can be found via formula 4.1.1 and 4.1.2:

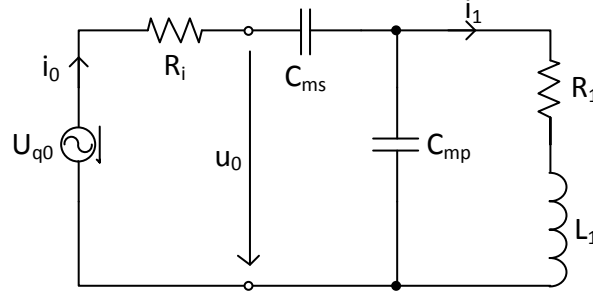


Figure 4.1: Equivalent circuit of a PCD

$$C_{mp} = \frac{R_i w L_1 - \sqrt{-R_i^2 R_1^2 + R_i R^3 + R_i w^2 L_1^2 R}}{R_i w (R^2 + w^2 L_1^2)} \quad (4.1.1)$$

$$C_{ms} = \frac{-C_{mp}^2 w^2 R_1^2 - C_{mp}^2 w^4 L_1^2 + 2 C_{mp} w^2 L_1 - 1}{C_{mp} w^2 R_1^2 + C_{mp} w^4 L_1^2 - w^2 L_1} \quad (4.1.2)$$

The quality factor Q , of the PCD antenna, primarily depends on the serial resistor R_1 of the inductance L_1 . This resistor consists of the physical losses from the inductance L_1 and a serial resistor, which is used to lower the quality factor Q . This is typically necessary to ensure a certain bandwidth B for the data communication. The quality factor Q can be calculated through formula 4.1.3:

$$Q_{coil} = \frac{w_{res} \cdot L_1}{R_1} \quad (4.1.3)$$

Formula 4.1.4 to formula 4.1.8 points the way of the calculation for current i_1 . Current i_1 is required for the calculation of the induced voltage in the PICC, which is also depended

on the mutual inductance M of the coupled system.

The parallel resonance circuit consists of the coil L_1 and its serial resistor R_1 , which are parallel to the capacity C_{mp} . Its impedance is calculated through formula 4.1.4. Adding the impedance of the antenna to formula 4.1.4, leads to the impedance of the PICC as shown in formula 4.1.5. According to *Ohm's law*, the current \dot{i}_0 can be calculated by dividing the induced voltage U_{q0} through the calculated impedance \underline{Z}_{PCD} . Furthermore, the current \dot{i}_1 through the antenna can be evaluated via the *Kirchhoff's law* in formula 4.1.8, which is very important for the consideration of the coupled system.

$$\underline{Z}_p = \frac{R_1 + j w L_1}{j C_{mp} w R_1 - C_{mp} w^2 L_1 + 1} \quad (4.1.4)$$

$$\underline{Z}_{PCD} = \underline{Z}_p - \frac{j}{C_{ms} w} + R_i \quad (4.1.5)$$

$$\begin{aligned} &= \frac{R_1 + j w L_1}{j w C_{mp} R_1 - C_{mp} w^2 L_1 + 1} - \frac{j}{C_{ms} w} + R_i \\ &= \left(\frac{(1 - C_{mp} w^2 L_1) R_1 + C_{mp} w^2 L_1 R_1}{C_{mp}^2 w^2 R_1^2 + (1 - C_{mp} w^2 L_1)^2} + R_i \right) + \\ & j * \left(\frac{w L_1 (1 - C_{mp} w^2 L_1) - C_{mp} w R_1^2}{C_{mp}^2 w^2 R_1^2 + (1 - C_{mp} w^2 L_1)^2} - \frac{1}{C_{ms} w} \right) \end{aligned}$$

$$\dot{i}_0 = \frac{U_{q0}}{\underline{Z}_{PCD}} \quad (4.1.6)$$

$$\underline{u}_{Z_p} = \dot{i}_0 \cdot \underline{Z}_p \quad (4.1.7)$$

$$\dot{i}_1 = \frac{\underline{u}_{Z_p}}{R_1 + j w L_1} \quad (4.1.8)$$

4.2 Proximity Integrated Circuit Card (PICC)

The basic equivalent circuit of a PICC, as shown in figure 4.2, consists of an antenna, a capacitor C_{tune} and an impedance of the Chip, which can be represented as a parallel

connection of a resistor R_{chip} and a capacitor C_{chip} . The main function of the capacitor C_{tune} is the resonance frequency tuning to a defined value.

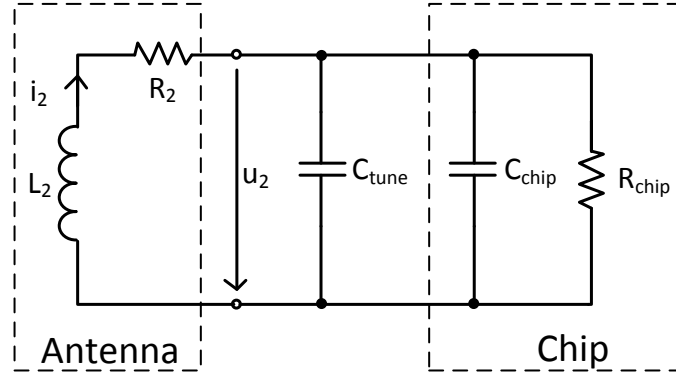


Figure 4.2: Basic equivalent circuit of a PICC

As the PICC is inductively coupled with the PCD, a voltage is induced in the antenna of the PICC. The voltage can thus be simplified seen as a serial voltage source to the inductance L_2 (illustrated in figure 4.3). The induced voltage is proportional to the mutual inductance, the operating frequency and the current i_1 in the PCD antenna (formula 4.2.1).

The equivalent circuit for the subsequently calculation is illustrated in figure 4.3. To simplify the calculation, capacitor C_{tune} and C_{chip} are added to capacitance C_2 .

Formula 4.2.2 specifies the impedance \underline{Z}_{PICC} , usually also known as \underline{Z}_T , which stands for the transponder impedance. The voltage u_2 largely corresponds to the supply voltage of the chip and is called in practice L_A - L_B voltage. According to phase resonance, the resonance frequency of the PICC can be calculated through formula 4.2.5.

$$\underline{U}_{q2} = j\omega M \cdot i_1 \quad (4.2.1)$$

$$\underline{Z}_{PICC} = j\omega L_2 + R_2 + \frac{R_L - j\omega C_2 R_L^2}{1 + R_L^2 \omega^2 C_2^2} \quad (4.2.2)$$

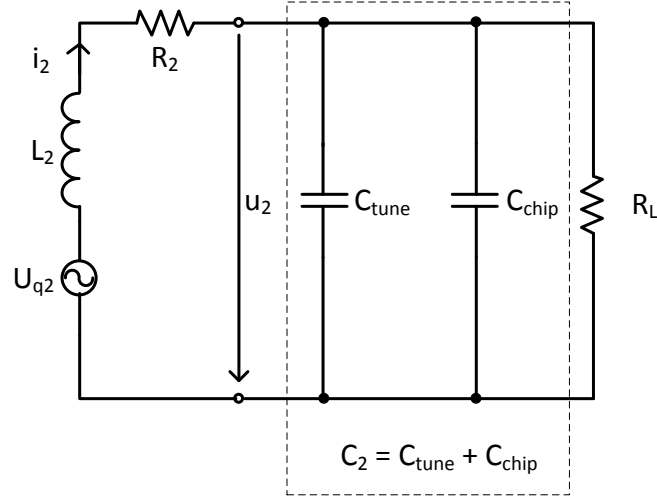


Figure 4.3: PICC equivalent circuit for calculation

$$= \left(\frac{R_L}{w^2 C_2^2 R_L^2 + 1} + R_2 \right) + j * \left(w L_2 - \frac{w C_2 R_L^2}{w^2 C_2^2 R_L^2 + 1} \right)$$

$$i_2 = \frac{U_{q2}}{\underline{Z}_{PICC}} \quad (4.2.3)$$

$$u_2 = i_2 * \left(\frac{R_L - jwC_2R_L^2}{1 + R_L^2w^2C_2^2} \right) \quad (4.2.4)$$

$$\Im \{ \underline{Z}_{PICC} \} \stackrel{!}{=} 0 \Rightarrow f_{res} = \frac{1}{2\pi} \cdot \sqrt{\frac{1}{C_2 L_2} - \frac{1}{R_L^2 C_2^2}} \quad (4.2.5)$$

Generally, a chip requires a DC voltage supply between 3 and 6 Volt (dependent on voltage class of chip) and therefore, the alternating voltage u_2 needs to be rectified. Figure 4.4 shows the equivalent circuit with a rectifier and shunt resistor. The rectification is usually done with a half wave or full wave rectifier. Additionally, the rectified voltage is smoothed by a smoothing capacitance. As mentioned before, the voltage u_2 is on the one hand dependent on the induced voltage U_{q2} , but on the other hand on the quality factor of the PICC resonance circuit. To achieve a constant voltage supply for the chip, the quality factor has to be regulated. Therefore, the parallel resistor R_{shunt} is variably

changed if the field strength varies. This mechanism guarantees a constant voltage level over a widely defined working range. According to Finkenzeller, the quality factor can be analytically represented through formula 4.2.6 [5]. If the field strength is very low, the quality factor of the PICC has to be high to gain enough energy from the magnetic field. This is usually the case, when the distance from the PICC to the PCD is at its maximum (under the consideration of the operating range). By bringing the PICC closer to the PCD, the field strength rises rapidly and therefore the induced voltage in the PICC rises rapidly too. The shunt mechanism detects this process and combats the rising voltage by reducing its shunt resistor to lower the quality factor.

In practice, the shunt resistor consists of several hundred resistors which are connected in parallel to each other. Typically, a resistance value range from 20 to 5000 Ohm is possible.

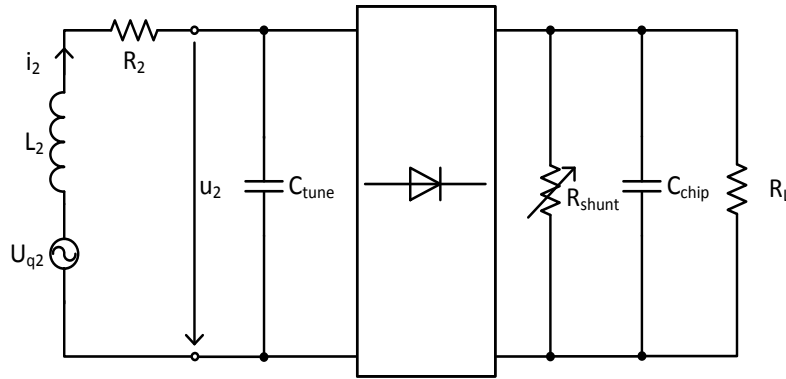


Figure 4.4: PICC equivalent circuit with rectifier and shunt resistor

$$Q_{PICC} = \frac{1}{R_2 \cdot \sqrt{\frac{C_2}{L_2}} + \frac{1}{R_L} \cdot \sqrt{\frac{L_2}{C_2}}} = \frac{1}{\frac{R_2}{wL_2} + \frac{wL_2}{R_L}} \quad (4.2.6)$$

Figure 4.5 illustrates the shunt mechanism related to the field strength H . Firstly, the shunt resistor is increased to get enough energy from the magnetic field. The maximal peak shows the point, where the PICC has enough energy for its voltage supply. At higher field strengths, it has to reduce the resistance as discussed before.

According to formula 4.2.6, the quality factor Q is illustrated in figure 4.6 for the values of the load resistor in figure 4.5. As shown in figure 4.6, the route of the quality factor

is equal to the route of the shunt resistor because the parameters L_2 , R_2 and w keep constant.

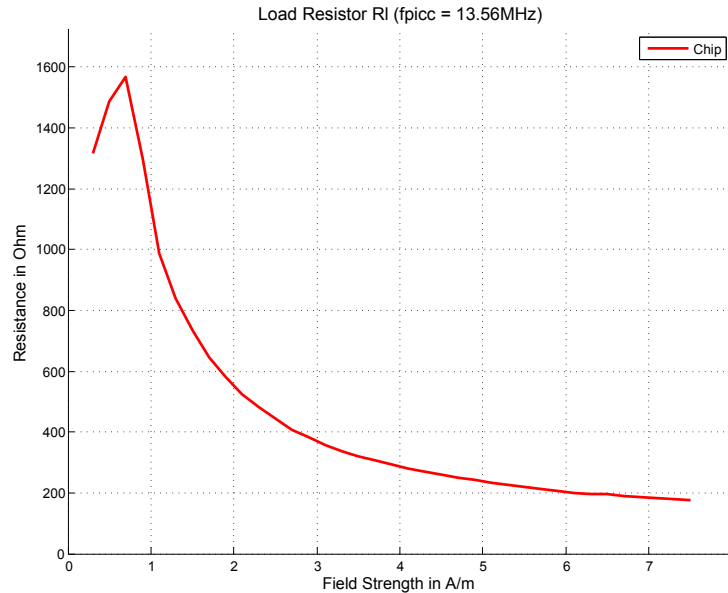


Figure 4.5: Shunt mechanism for voltage regulation

4.3 Transformed Transponder Impedance

PICC and PCD form a coupled RFID System, where the PCD is the active and the PICC the passive device. The mutual inductance M describes the intensity of the connected devices. It can be measured with a network analyzer by evaluating the S-parameters of the two port network. Through these parameters, it is possible to calculate the inductance values L_1 , L_2 and their mutual inductance M . It is important that consideration is given to the correct measurement of the values, because they are very important for additional calculation and for the dimensioning of the system. It should also be noted, that the measurement is only done with the inductances and without any additional wiring. If additional connections to the inductances are needed, they have to be compensated by the compensation option of the network analyzer.

Figure 4.7 illustrates the coupled RFID system, which consists on the left side of the PCD and on the right side of the PICC. The circuit at the bottom of the figure shows the equivalent circuit for this system, where the PICC can be represented as the transformed

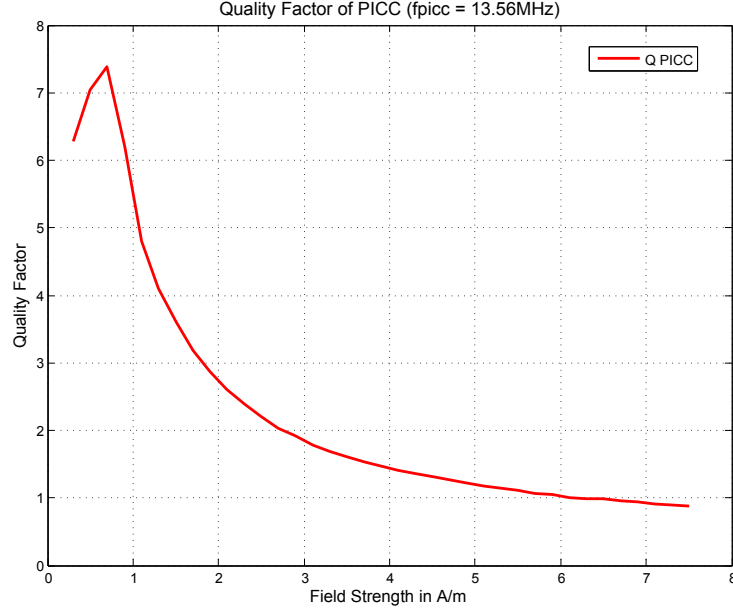


Figure 4.6: Quality factor of PICC

transponder impedance Z'_T . As shown in formula 3.5.4, the PICC is able to influence the PCD through its current i_1 . That means, that the PICC can be seen as a load for the PCD in its antenna circuit. According to Finkenzeller [5], the transformed transponder impedance can be calculated as following:

$$\underline{Z}'_T = \frac{w^2 k^2 \cdot L_1 \cdot L_2}{\underline{Z}_{PICC}} = \frac{w^2 k^2 \cdot L_1 \cdot L_2}{jwL_2 + R_2 + \frac{R_L - jwC_2 R_L^2}{1 + R_L^2 w^2 C_2^2}} \quad (4.3.1)$$

The PCD is called unloaded, if the PICC is not in the operating range of the PCD, which means that the coupling factor k is zero. Nevertheless, a constant current i_1 is passing through the antenna of the PCD, dependent on the quality factor of the PCD and its supply voltage. As mentioned before, the PICC can be represented as a load for the PCD, if it is brought into the operating range of the PCD. Consequently, the current i_1 decreases, due to the damping of the quality factor of the PCD by Z'_T . This effect is called *loading* and shall not be reduced to a certain value, which is specified in the related ISO standard 10373-6 [8]. The current i_1 for the unloaded state can be calculated through formula 4.1.8.

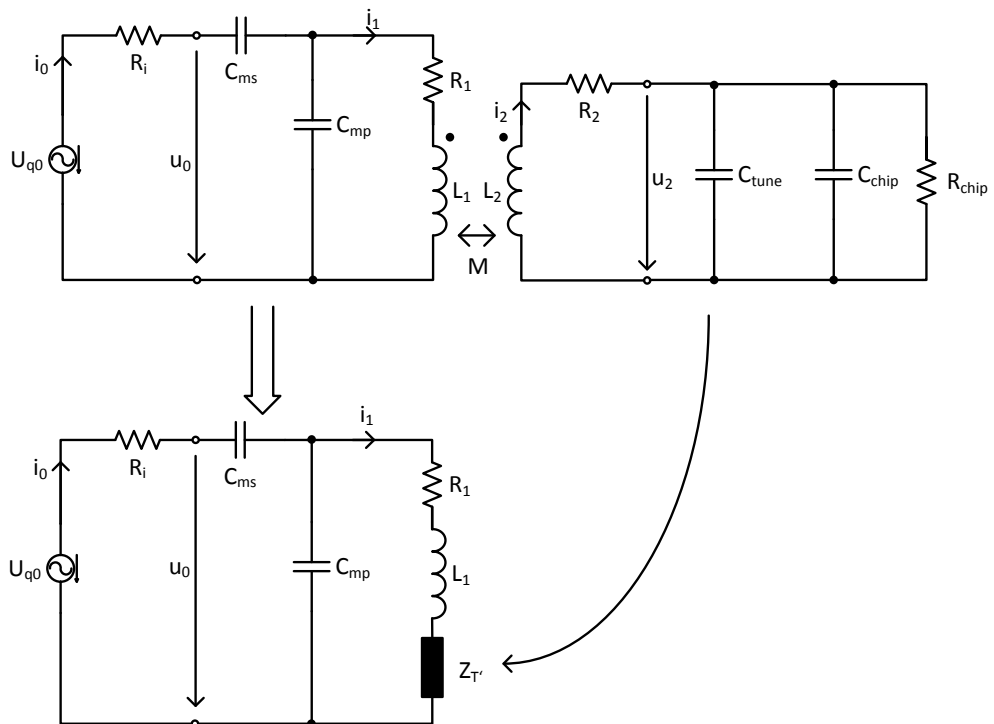


Figure 4.7: Equivalent circuit for transformed transponder impedance

The current for the loaded state can be calculated in the same way:

$$\underline{Z}_{p_i} = \frac{\underline{Z}'_T + R_1 + j w L_1}{\underline{Z}'_T j w C_{mp} R_1 + j C_{mp} w R_1 - C_{mp} w^2 L_1 + 1} \quad (4.3.2)$$

$$\underline{Z}_{PCD_i} = \underline{Z}_{p_i} - \frac{i}{C_{ms} w} + R_i \quad (4.3.3)$$

$$i_{0_i} = \frac{U_{q0}}{\underline{Z}_{PCD_i}} \quad (4.3.4)$$

$$\underline{u}_{Z_{p_i}} = i_{0_i} \cdot \underline{Z}_{p_i} \quad (4.3.5)$$

$$i_{1_i} = \frac{\underline{u}_{Z_{p_i}}}{R_1 + i w L_1 + \underline{Z}'_T} \quad (4.3.6)$$

Figure 4.8 illustrates the transformed transponder impedance of a chip as a function of the distance to the PCD (corresponds to a coupling factor k from 0 to 0.17). The impedance \underline{Z}'_T increases as the square progression of the coupling factor k , which increases by approaching the PICC to the PCD. Figure 4.9 shows the effect to the reader antenna current i_1 , which is known as the *loading effect*. The marked point at the right bottom represents the current vector when the coupling factor is zero. The phase shift of the current is related to the phase of the voltage source U_{q0} . A higher transformed impedance leads to a lower absolute value of the current in the antenna of the PCD. As the transformed transponder impedance is not only real valued, a small phase shift is caused too.

4.4 Data Communication

The previous sections of this master's thesis, briefly describe the construction of the RFID system and the electrical and mathematical description of its parts. In some cases it was shown, how the PCD can be influenced by the PICC. Finally, this chapter covers the digital data communication between a PCD and the PICC.

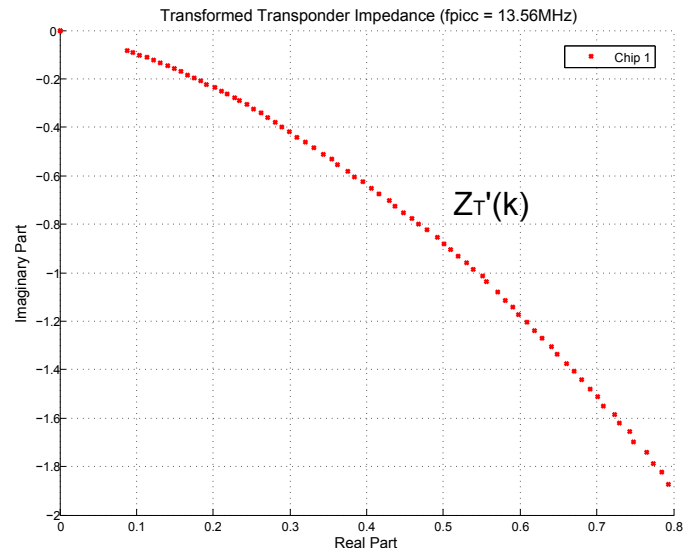


Figure 4.8: Transformed transponder impedance as a function of the coupling factor

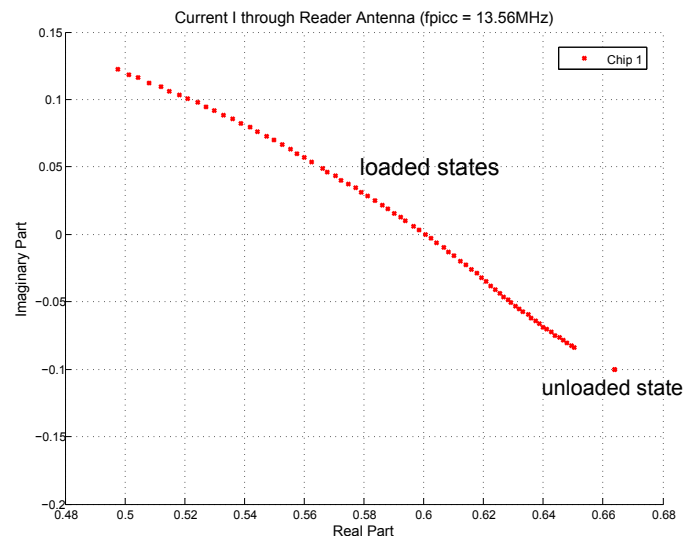


Figure 4.9: PCD antenna current as a function of the transformed transponder impedance

4.4.1 Communication from PCD to PICC

On the one hand, the PCD has to supply the PICC with energy through its magnetic field, but on the other hand, the PCD is able to send data to the PICC by changing the magnetic field in time. Since the PICC needs energy for a proper work of its system, the PCD is just allowed to switch the magnetic field for a short time off. Generally, the modulation for the downlink (PCD to PICC) can be realized with ASK (Amplitude Shift Keying), FSK (Frequency Shift Keying) or PSK (Phase Shift Keying). The most popular types are ASK and PSK because their demodulation can be implemented very easily [12]. According to the ISO/IEC 14443 standard for proximity cards, the modulation is realized with an ASK modulation.

There are two modulation types specified in ISO/IEC 14443 [6]:

- **Type A:** ASK, 100% modulation index, Modified Miller
- **Type B:** ASK, 10% modulation index, NRZ

The carrier frequency for the ASK modulation is at 13.56 MHz. Additionally, a data rate of 106 kbit/s (13.56 MHz/128), 212, 424 and 848 kbit/s is specified in ISO/IEC 14443 [6]. Furthermore, an anticollision algorithm must be implemented to avoid a possible data collision of more than one PICC in the operating range of the reader. Another specified point is that the reader acts as the master and therefore has to start the talk according to the protocol principle.

Basically, a double sideband amplitude modulation can be mathematically defined through formula 4.4.1 [4]. f_c is the center frequency or carrier frequency and its value is always 13.56 MHz. f_m is the modulation frequency and it is dependent on the specified data rate. As the system uses ASK, formula 4.4.1 for AM changes to formula 4.4.3. The function $A(t)$ stands for the transmitted binary bits, where one bit can be 0 or 1.

Figure 4.11 and 4.10 show a bit stream of an ASK modulated signal with a 13.56 MHz carrier and 847.5 kHz subcarrier. As illustrated in figure 4.10, the magnetic field is turned off if a zero bit occurs. However, it may happen that several zeros immediately follow in a sequence and this would mean, that the PICC has no energy for the hole time of the zero-sequence. NRZ (non-return-to-zero) coding will therefore not be used for the *Type A* modulation. Instead, modified miller coding is used, which guarantees that the low states are very short (illustrated in figure 4.12).

$$s(t) = [K + a \cdot \cos(2\pi f_m t)] \cdot \cos(2\pi f_c t) \quad (4.4.1)$$

The modulation depth m is defined as [4]:

$$m = \frac{\text{modulating signal amplitude}}{\text{unmodulated carrier amplitude}} = \frac{a}{K} \quad (4.4.2)$$

$$s(t) = A(t) \cdot \cos(2\pi f_c t) \quad (4.4.3)$$

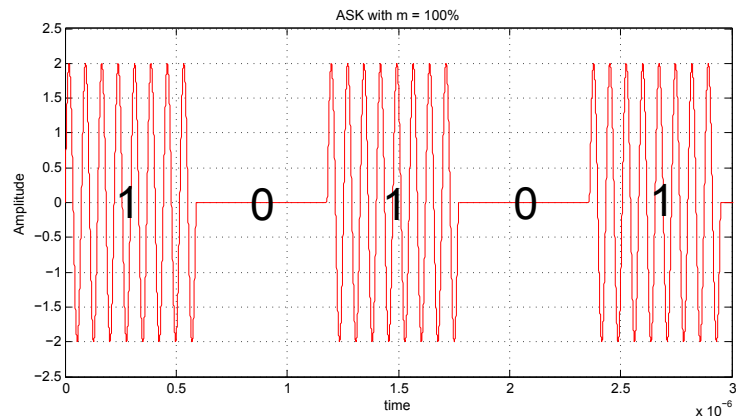


Figure 4.10: ASK with 100% modulation index, NRZ coding

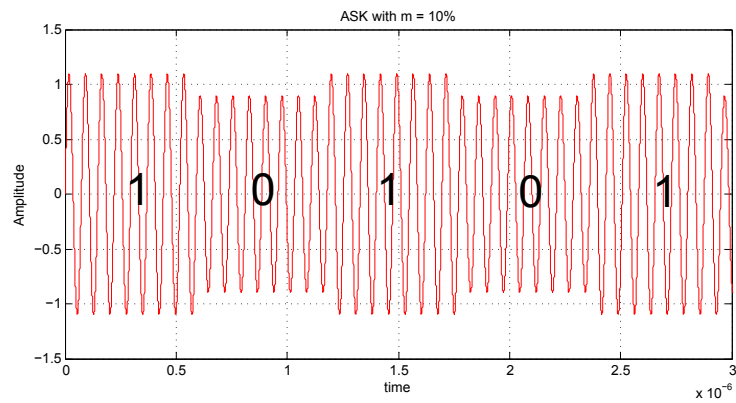


Figure 4.11: ASK with 10% modulation index, NRZ coding

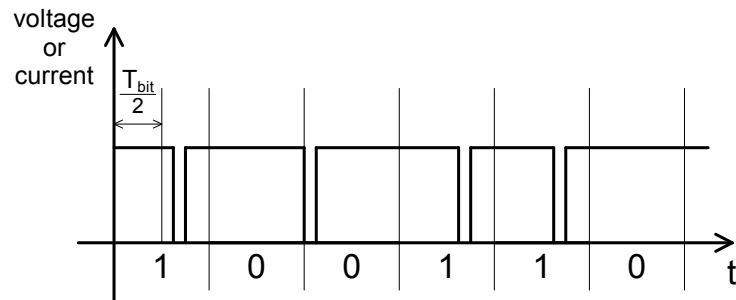


Figure 4.12: Modified Miller coding [11]

4.4.2 Communication from PICC to PCD

In the previous sections it was shown, how the impedance of the PICC can influence the PCD. The PICC is able to reduce the current in the antenna of the PCD via the transformed transponder impedance Z'_T . Basically, there are two opportunities for changing the PICC impedance Z_T :

- Ohmic load modulation (figure 4.13)
- Capacitive load modulation (figure 4.14)

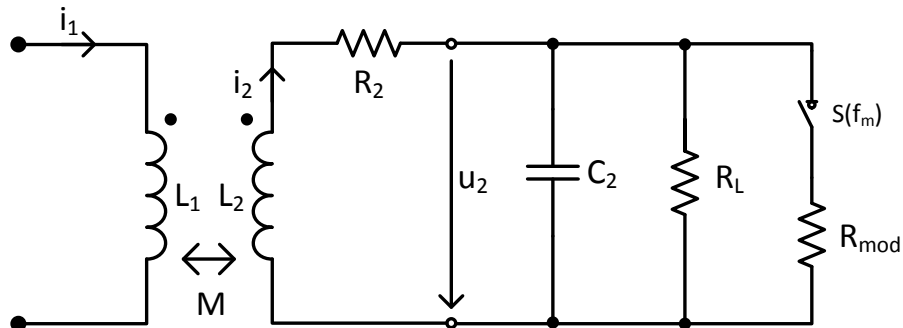


Figure 4.13: Ohmic load modulation

In both modulation cases the load of the PICC is alternated with the subcarrier frequency and according to its binary data stream. Both load modulation methods conform to an amplitude modulation (AM). The further investigations are based on the ohmic load modulation because this is the common method in practice. The principle of the ohmic load modulation allows an easier implementation as the capacitive load modulation in a chip because it can be combined with the shunt mechanism.

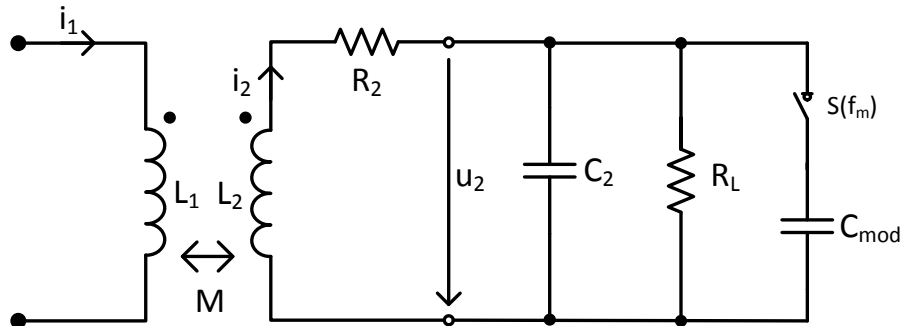
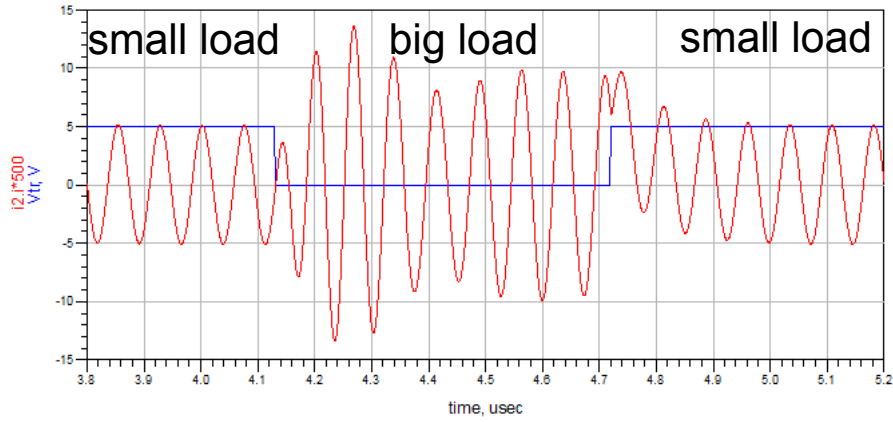


Figure 4.14: Capacitive load modulation

The parallel resistor and capacitor influence the resonance frequency of the PICC and therefore, the resonance frequency will be changed by the alternating load modulation. Moreover, it must not be forgotten that the value of the resistor R_L in figure 4.13 is just constant for a certain distance to the PCD. Changing the distance or field strength will result in a change of the resistors value because of the shunt mechanism. The load modulation leads to a change of the PICC impedance and further to a change of the current i_2 , which plays a decisive role for the data communication. The effect of an ohmic load modulation, according to the current i_2 in the PICC antenna, is shown in figure 4.15. The signal v_{tr} stands for the voltage at the switch $S(f_m)$, which switches the resistor R_{mod} parallel to the load resistor R_L . It results in a smaller parallel resistor of the resonance circuit and the current i_2 is decreased because the quality factor is decreased too, and therefore, less energy can be transferred from the PCD to the PICC. As this system of resonance circuits is dynamic, the change of the current i_2 between the two states requires a certain time and leads to a current overshoot and undershoot. Overshoot, undershoot, rise and fall time of the current are mainly dependent on the value difference of the shunted resistor values. Ultimately, this means that the quality factor Q of the PICC is extremely modified. On the one hand, a major variation of the quality factor leads to a higher change of the current i_2 , which is desirable for data communication, but on the other hand, it has a negative impact on the overshoot and undershoot behavior.

Furthermore, the load modulation influences not only the magnitude of the current i_2 , it has an impact on the phase too. As a result, the load modulation can be seen as a combination of an amplitude and phase modulation (formula 4.4.4 and 4.4.5). When the events are considered in their entirety, the two resulting states of the current i_2 can

Figure 4.15: Current i_2 according to load modulation

be represented in a polar diagram according to its magnitude and phase (illustrated in figure 4.16).

Amplitude Shift Keying (ASK):

$$s_{ASK}(t) = A(t) \cdot \cos(2\pi f_c t + \varphi_0) \quad (4.4.4)$$

Phase Shift Keying (PSK):

$$s_{PSK}(t) = A_0 \cdot \cos(2\pi f_c t + \varphi(t)) \quad (4.4.5)$$

Impedance of PICC for unmodulated state:

$$\underline{Z}_{PICC,unmod} = j\omega L_2 + R_2 + \frac{R_L - j\omega C_2 R_L^2}{1 + R_L^2 \omega^2 C_2^2} \quad (4.4.6)$$

$$\dot{i}_{2,unmod} = \frac{U_{q2}}{\underline{Z}_{PICC,unmod}} \quad (4.4.7)$$

$$\underline{Z}'_{T,unmod} = \frac{\omega^2 k^2 \cdot L_1 \cdot L_2}{\underline{Z}_{PICC,unmod}} \quad (4.4.8)$$

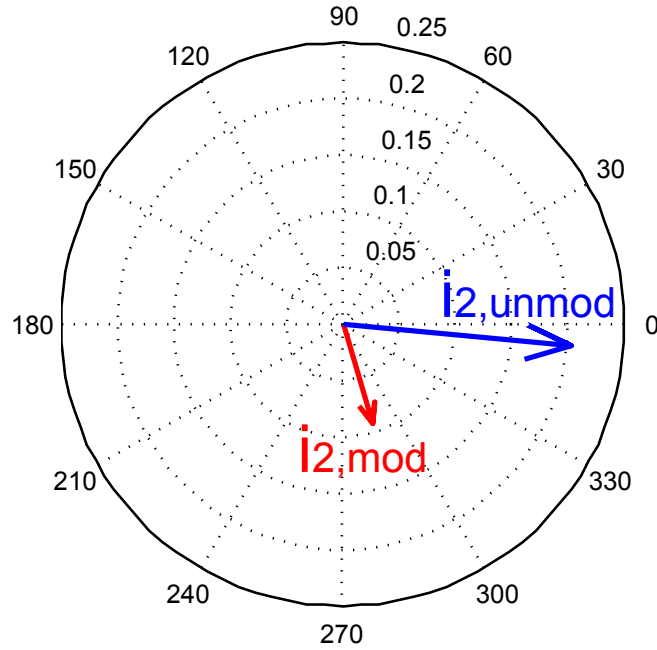


Figure 4.16: Pointer diagram of the modulated states of i_2 (example)

Impedance of PICC for modulated state:

$$\underline{Z}_{PICC,mod} = j\omega L_2 + R_2 + \frac{R_L \cdot R_{mod}}{R_L + R_{mod} + j\omega C_2 \cdot R_L \cdot R_{mod}} \quad (4.4.9)$$

$$i_{2,mod} = \frac{\underline{U}_{q2}}{\underline{Z}_{PICC,mod}} \quad (4.4.10)$$

$$\underline{Z}'_{T,mod} = \frac{\omega^2 k^2 \cdot L_1 \cdot L_2}{\underline{Z}_{PICC,mod}} \quad (4.4.11)$$

Figure 4.17 illustrates the load modulated current i_2 in its frequency domain. The highest part in the plot is the carrier at the frequency f_c of 13.56 MHz. Additionally, the remaining frequency parts indicate the rectangular wave shape of the subcarrier with a frequency f_m of 847.5 kHz.

The Fourier series of a rectangular wave shape is defined in formula 4.4.12 [3]:

$$f(x) = \frac{4h}{\pi} \cdot \left(\sin(x) + \frac{1}{3}\sin(3x) + \frac{1}{5}\sin(5x) + \frac{1}{7}\sin(7x) + \dots \right) \quad (4.4.12)$$

$$x = w \cdot t$$

Formula 4.4.12 represents the rectangular wave shape in time domain. By transforming it with the Fourier transformation to the frequency domain, the separated sinus components with the uneven number of subcarrier frequencies can be illustrated. It should be noted, that a sine wave form in time domain is a peak in frequency domain. Because of the general characteristics of amplitude modulation, the peaks of the transformed sinus signals are theoretically symmetric to the carrier frequency f_c .

It is important to say, that the magnitude of the subcarriers in the amplitude spectrum are dependent on amplitude and phase modulation. Therefore, a PSK modulated signal has a magnitude in the amplitude spectrum! This example is shown in figures 4.18 and 4.19.

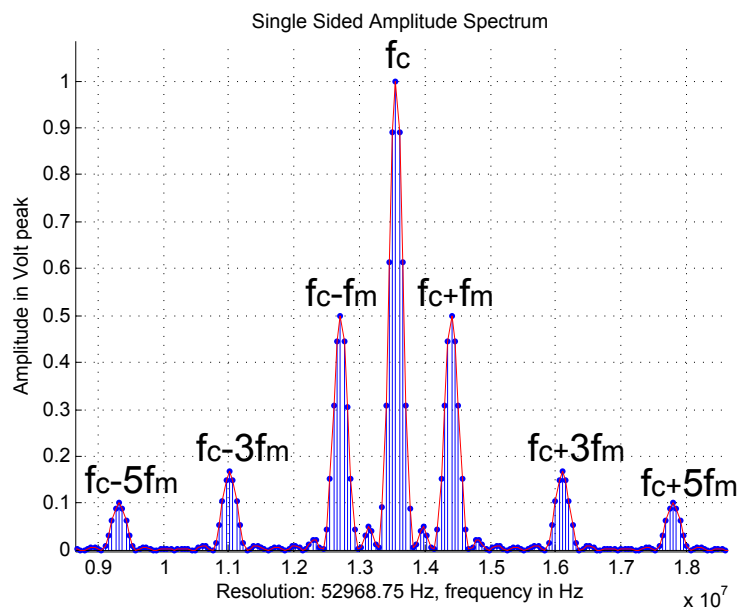


Figure 4.17: Spectrum of load modulation

Optimal Switching Point:

As already mentioned, the load modulation switch $S(f_m)$ alternates the two load resistor

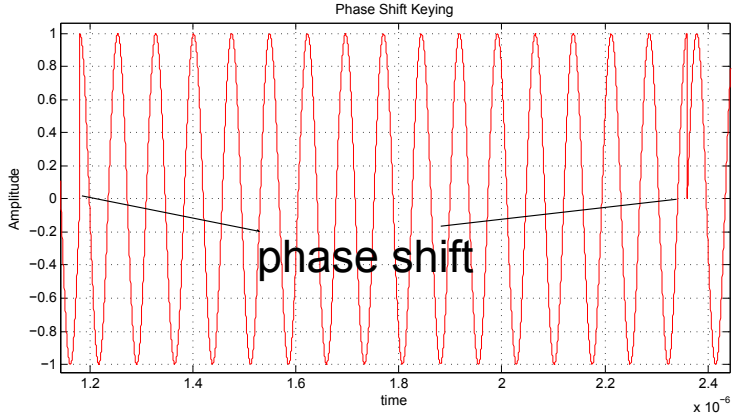


Figure 4.18: PSK modulated signal

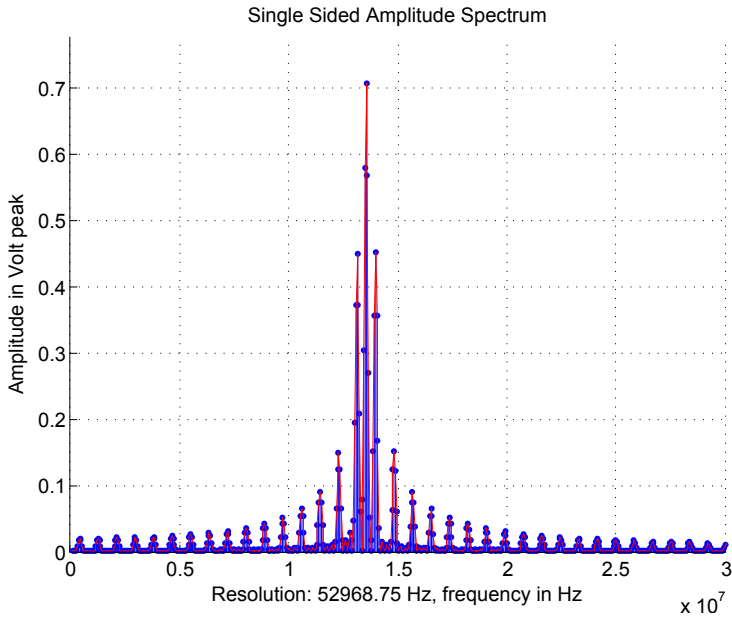


Figure 4.19: Spectrum of PSK modulated signal

values with the subcarrier frequency f_m . The question is whether, how the switching time point influences the modulated signal according to the carrier signal. By means of the simulation of the RFID model, with the simulation program *Advanced Design Services* (ADS), it could be shown, that the switching time has different consequences to the overshoot and undershoot behavior of the current i_2 . As discussed earlier, a larger change of the resistor values leads to a higher overshoot and undershoot of the antenna current i_2 . On the basis of chip measurements, it was determined, that this problem occurs especially at higher PICC resonance frequencies and lower field strengths.

Figure 4.20 illustrates the simulation results of two different switching time points with reference to the carrier frequency. In both cases the same load resistor values are switched. The left picture represents the alternating current i_2 , when it is switched in its null walk through. The current, in the figure on the right side, is switched at its highest point. We can see, that the overshoot and undershoot behavior is worse than in the right figure, which means, that the switching point from current i_2 at its maximum has a negative consequence to the overshoot and undershoot behavior of the signal. Experimental measurements of a standardized PICC validate the simulation results, as illustrated in figure 4.21. The figure represents the overshoot as the continuous line and the undershoot as the dashed line over the phase shift from the rectangular subcarrier signal to the carrier signal. In addition, it could be measured that the minimal points are at the null walk through of the alternating current, as already found out in the simulation. Further investigations have shown, that the overshoot can be reduced by up to 30% in comparison to the worst case behavior!

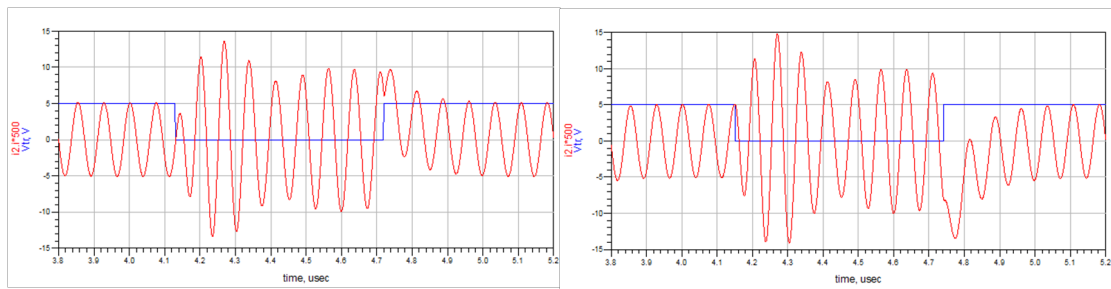


Figure 4.20: Switching point of load modulation regarding to overshoot/undershoot

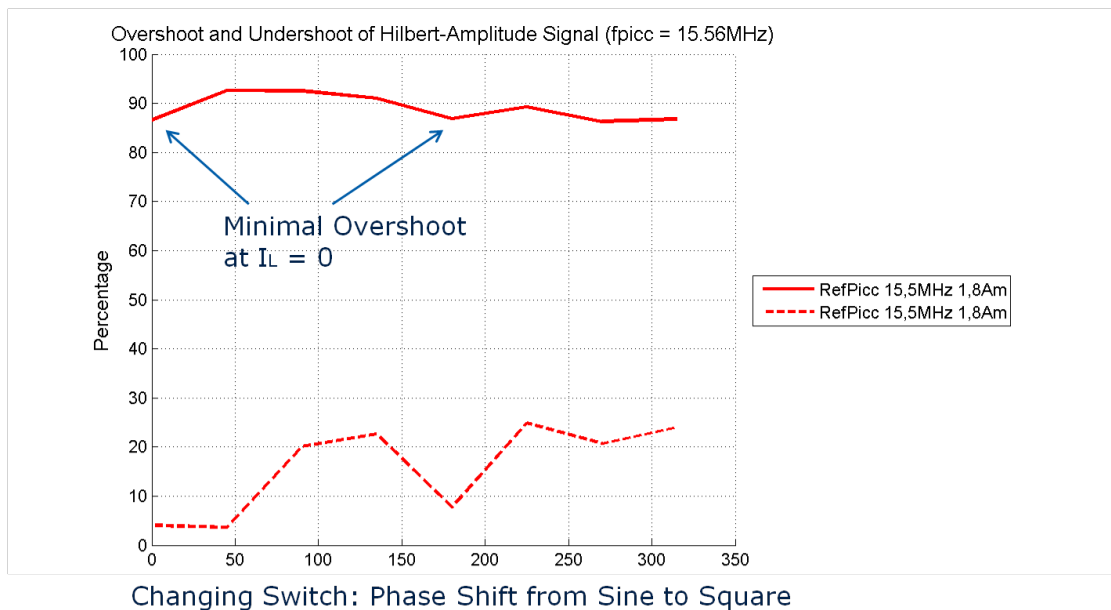


Figure 4.21: Overshoot/undershoot of i_2 related to switching point

Chapter 5: Standardized Measurement Methods

Generally, RFID standards and regulations describe the guidelines and laws that must be complied for RFID products.

- **Regulative Norms [6]:**
Defines the general permission for the radiation of radio waves in the frequency band for applications. Following measurement methods and limits are defined:
 - Frequency spectrum
 - Power
 - Duty cycle
 - Listen before talk
 - etc.
- **Product Standards [6]:**
Defines under the regulatory authorization, how a specific RFID system works. E.g.:
 - Carrier frequency
 - Transmission power
 - Type of modulation
 - Data rate
 - Channel coding
 - Commands for communication
 - Anti-collision mechanism
 - Data encryption

5.1 ISO Set-up

ISO stands for the *International Organization for Standardization* and ICE for the *International Electrotechnical Commission*. ISO/IEC 14443 is the standard for contactless integrated proximity identification cards and defines the physical characteristics, radio frequency power, signal interface, initialization, anticollision and transmission protocol in four parts. ISO/IEC 10373-6 describes the test methods for proximity identification cards and is cross-referenced to many base standards. This master's thesis deals with the measurement of load modulation and the loading effect. However, other detailed points from the specification of proximity cards have not been investigated.

5.1.1 VLMA

VLMA stands for *Voltage Load Modulation Amplitude* and it can be measured with the ISO test set-up. The value of the VLMA provides information about the effectiveness of the load modulation in the PICC. Typically, VLMA values are calculated by the discrete Fourier transformation over six cycles of the modulated current i_2 . Moreover, the transformation displays the modulated signal in its frequency domain and the two VLMA values are the levels at the frequency points $f_t + f_m$ and $f_t - f_m$ in volt peak, which are known as the upper and lower sideband (figure 5.1) [8] [7].

Furthermore, the limits for the minimal VLMA values are defined in ISO/IEC 14443 and they are dependent on the adjusted field strength. Considering the measurement of the VLMA values, the operating field strength is defined in a range between 1.5 A/m (H_{min}) and 7.5 A/m (H_{max}). Mathematically, the minimal VLMA values for the PICC and PCD are defined as following [7]:

$$V_{LMA,PICC} = \frac{22}{\sqrt{H}} \quad (5.1.1)$$

$$V_{LMA,PCD} = \frac{18}{\sqrt{H}} \quad (5.1.2)$$

Formula 5.1.1 specifies the minimal value for both VLMA levels, which must be achieved by load modulation. Formula 5.1.2 specifies the minimum VLMA values, which must be correctly interpreted by the PCD. Limits for the minimum load modulation amplitude are illustrated in figure 5.2 as a function over the defined operating field strength [7].

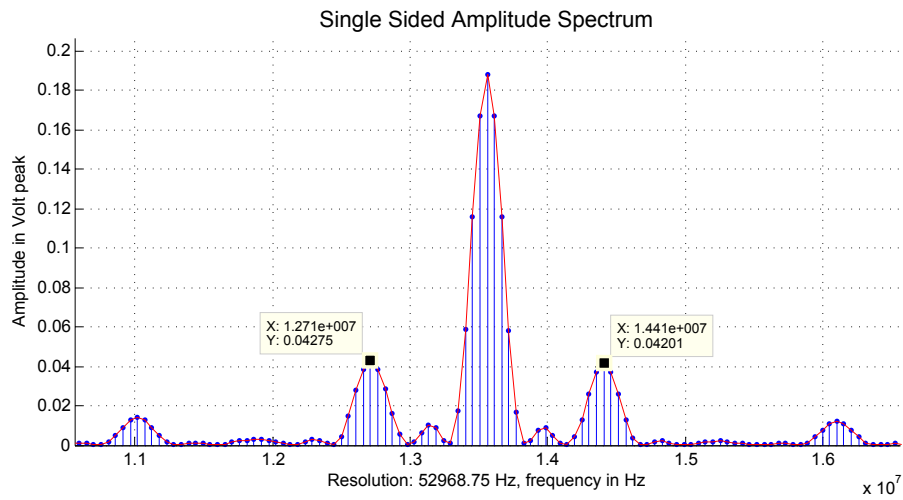


Figure 5.1: VLMA Measurement: Values at upper and lower sideband [2]

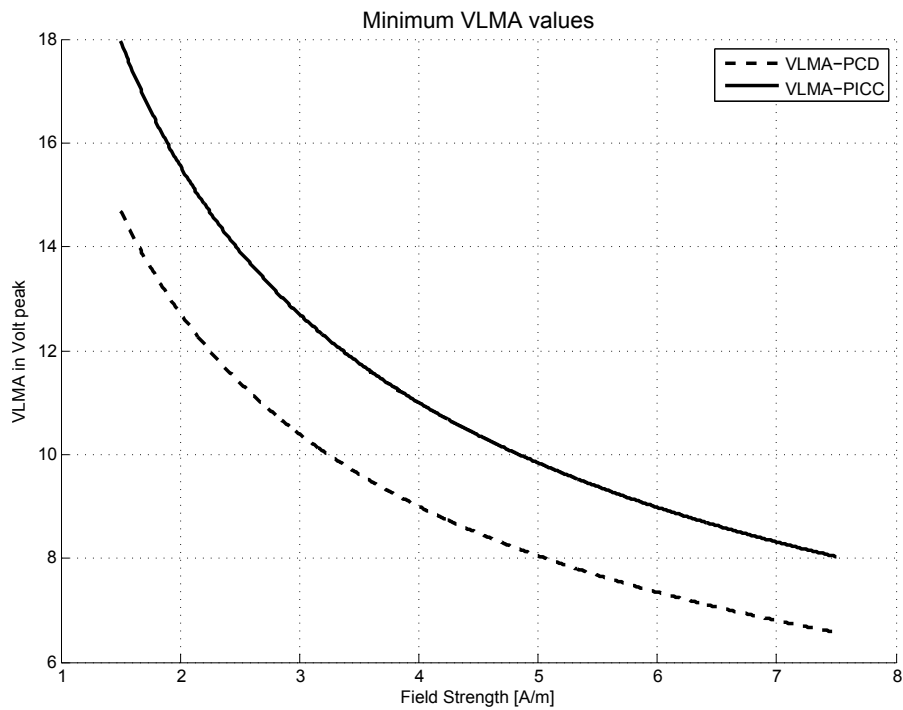


Figure 5.2: Minimum VLMA values according to ISO/IEC 14443 [7]

5.1.2 Test Set-up

Figure 5.3 illustrates the ISO-Measurement set-up for proximity cards according to ISO/IEC 10373. Main part of the set-up is the three-stage tower. In the middle of the tower is the main coil of the PCD, which creates the magnetic field, and the additional circuit for the measuring bridge. Furthermore, the first and third stage of the tower consist of a sense coil and belong to the measuring bridge. On the top of the stage is the measurement object (PICC) placed. And in addition, a calibration coil is mounted at the bottom of the last stage for field strength measurement (illustrated in figure 5.4). It is important to say, that the signals must be measured with high impedance RF-probes and additionally, they should have a low internal capacitance (smaller than 14 pF). With the help of the test set-up, the measurement of the differential voltage at the bridge, which is proportional to current i_2 , is realized. Basically, the coupling factor from the PCD to the calibration coil is equal to the coupling factor from the PCD to the PICC because both have the same layout (ID-1 card) and distance to the reader coil. Figure 5.4 represents the general principle of the ISO tower. *Sense coil A* and *sense coil B* are passed by the same flux density B , that means, that the same voltage level is induced in both coils. The measuring bridge displays zero differential voltage u_d in that case. When a PICC is placed on the ISO tower, and the PCD is driven by an alternating current, the PICC antenna coil causes a magnetic flux, which counteracts to the magnetic flux of the PCD. In that case, the recognized magnetic flux by *sense coil A* is reduced. As a consequence, the induced voltage in *sense coil A* and *sense coil B* is unequal and the measuring bridge indicates the voltage difference of both. With the help of this principle, one is able to measure only the impact of the PICC because the effect of the PCD is eliminated through the subtraction.

Figure 5.5 illustrates the principle of the measuring bridge in the ISO-tower, which is built up by the first and the third stage. Accordingly, figure 5.6 shows the electrical equivalent circuit of the measuring bridge. U_{qA} and U_{qB} represent the induced voltage in the two sense coils and are ideally equal if there is no PICC in the operating range. u_d stands for the measured differential voltage by the oscilloscope and R_{Probe} and C_{Probe} are the internal impedance values of the probe. Ideally, the inductance values $L_{sense,A}$, $L_{sense,B}$ and the coupling factor from the main coil to the sense coils are equal. In practice, this idealized case is not reachable because the values for the inductances are manufacturing depended. Secondly, the tower is not entirely symmetric and therefore, the coupling

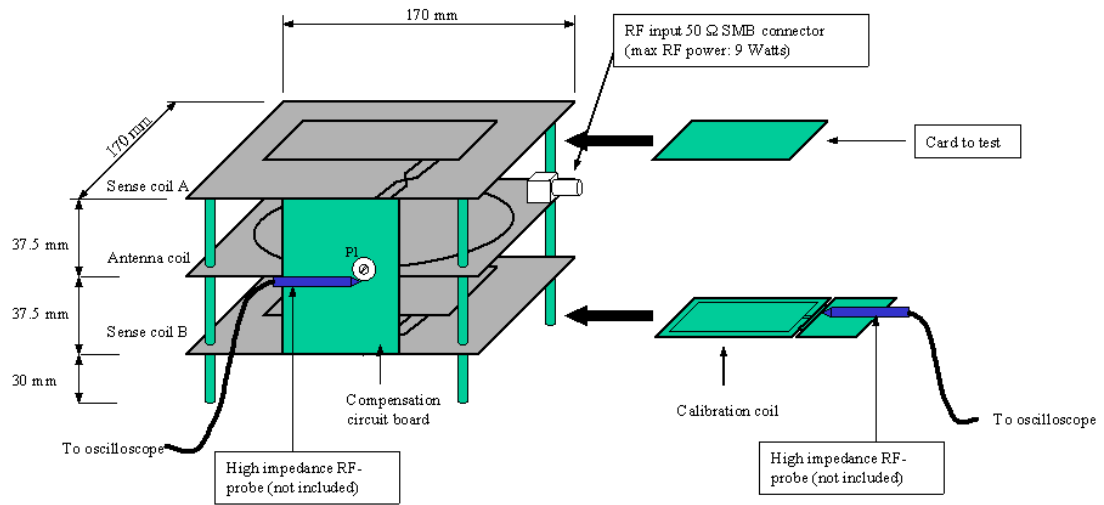


Figure 5.3: ISO-Measurement set-up [2]

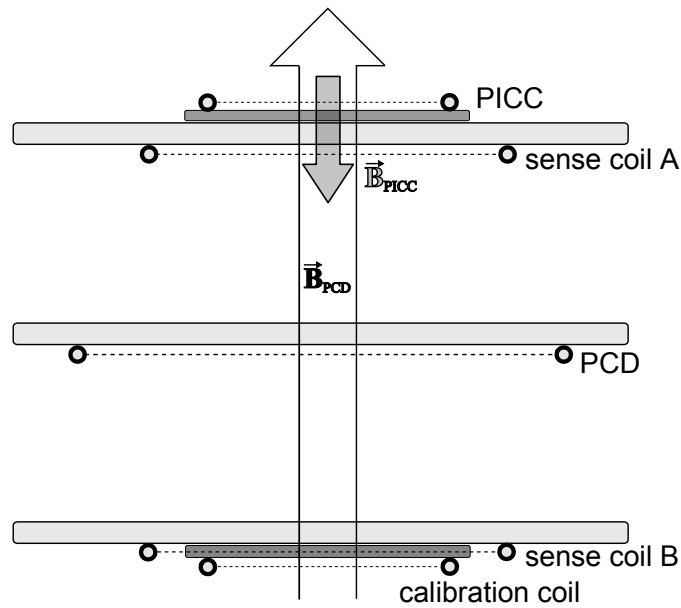


Figure 5.4: Cross section of ISO-Tower

Part	Value
$L_{sense,A}, L_{sense,B}$	375 nH
L_{PCD}	495 nH
L_{PICC} (4 coil turns, ID1)	2.3 μH
L_{PICC} (3 coil turns, ID1)	1.45 μH
L_{PICC} (2 coil turns, ID1)	0.76 μH
L_{CAL} (without feed line)	230 nH
$R_{i,A}, R_{i,B}$	0.65 Ω
$R_{i,PCD}$	0.8 Ω
$R_{i,PICC}$	1.8 Ω
$k_{PCD,A}, k_{PCD,B}$	0.0929
$k_{PCD,PICC}, k_{PCD,CAL}$	0.0505
$k_{PICC,A}$	0.1716
$k_{PICC,B}$	0.0161

Table 5.1: Values for ISO-Tower

factors are not the same. In view of further investigations, this undesirable alternating voltage is called error vector or error voltage u_{error} .

Table 5.1 illustrates the measured values for the ISO set-up.

Current i_d can be calculated by solving the following three equations:

$$I : 0 = -\underline{U}_{qA} + \underline{i}_A \cdot (j\omega L_{sense,A} + 145\Omega + R_{i,A}) + \underline{i}_d \cdot \frac{R_{Probe}}{j\omega C_{Probe} \cdot R_{Probe} + 1} \quad (5.1.3)$$

$$II : 0 = -\underline{U}_{qB} + \underline{i}_B \cdot (j\omega L_{sense,B} + 145\Omega + R_{i,B}) - \underline{i}_d \cdot \frac{R_{Probe}}{j\omega C_{Probe} \cdot R_{Probe} + 1} \quad (5.1.4)$$

$$III : \underline{i}_d = \underline{i}_A - \underline{i}_B \quad (5.1.5)$$

$$\underline{u}_d = \underline{i}_d \cdot \frac{R_{Probe}}{j\omega C_{Probe} \cdot R_{Probe} + 1} \quad (5.1.6)$$

As the explicit solution for i_d is quite long and complex, it is not specified.

The induced voltages U_{qA} and U_{qB} consist of the magnetic flux parts from the PCD and PICC. Ideally, the part from the PICC should be high for U_{qA} and zero for U_{qB} . But this is not reachable in practice, as you can see in table 5.1 according to the coupling factor values. The error voltage can be minimized by calibrating the 10 Ohm potentiometer. However, it is only possible to compensate the real part of the error vector and not the

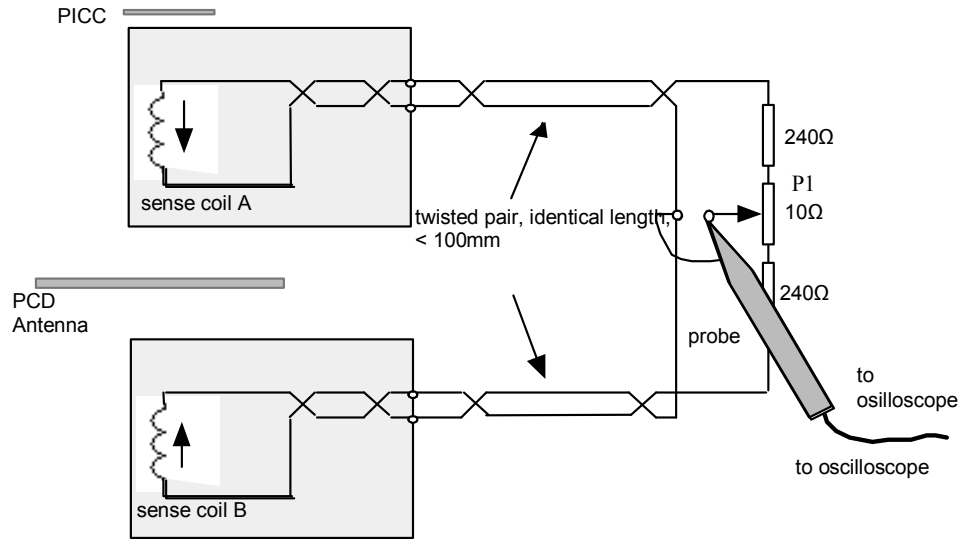


Figure 5.5: Bridge connection of ISO-tower [2]

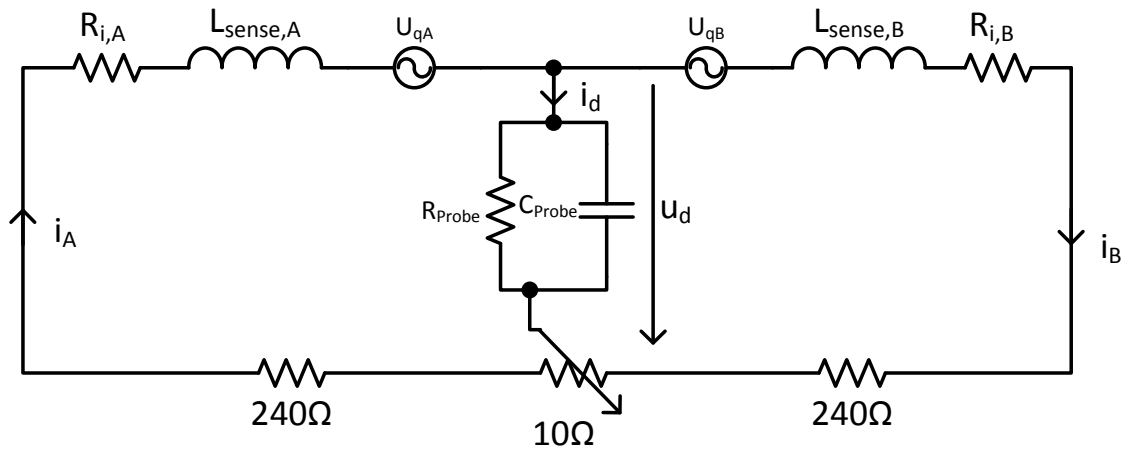


Figure 5.6: Electrical equivalent circuit of the measuring bridge [2]

hole imaginary part. Generally, the error vector has to be smaller than 50 mV at a field strength of 1.5 A/m. Figure 5.7 illustrates the compensation of the error vector through the variation of the potentiometer (P_1 in figure 5.5). R_1 stands for the resistance in one part of the bridge and consists of the 240 Ohm resistor, R_i and the part of the potentiometer. Basically, the compensation of different inductance values works in a similar way. Moreover, it can be shown, that the magnitude and phase of the error vector is frequency dependent (illustrated in figure 5.8).

The consideration of the error vector is very important because otherwise it has negative effects on the measurement of the current in phase and magnitude.

$$\underline{U}_{qA} = j\omega M_{PCD,A} \cdot \underline{i}_1 - j\omega M_{PICC,A} \cdot \underline{i}_2 \quad (5.1.7)$$

$$\underline{U}_{qB} = j\omega M_{PCD,B} \cdot \underline{i}_1 - j\omega M_{PICC,B} \cdot \underline{i}_2 \quad (5.1.8)$$

$$M_{picc,A} \gg M_{picc,B}$$

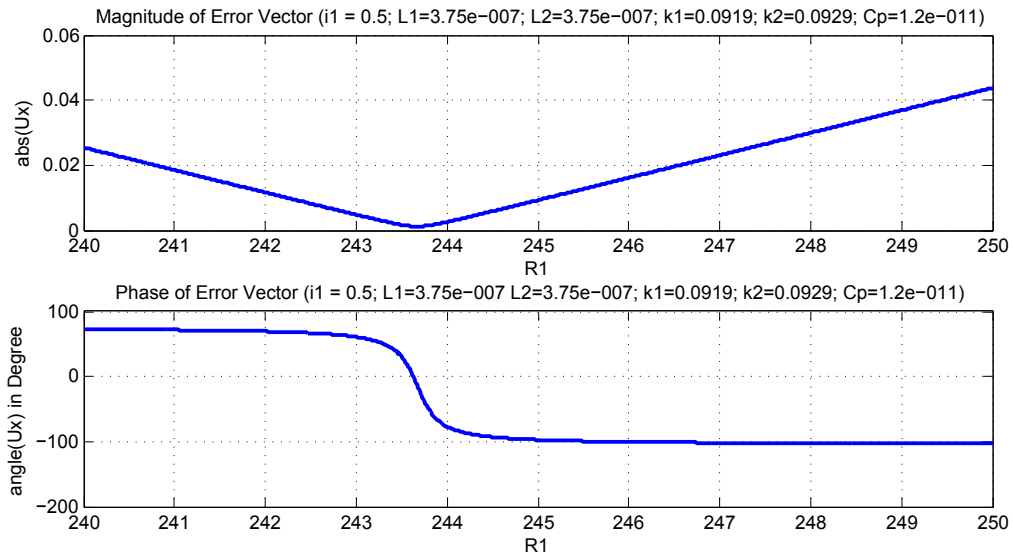


Figure 5.7: Compensation of error voltage with potentiometer

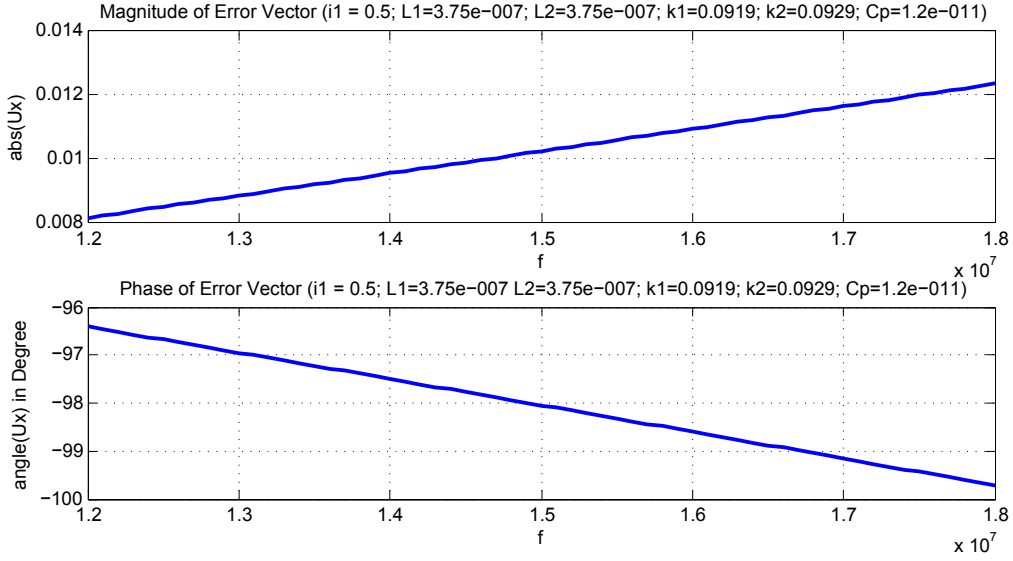


Figure 5.8: Frequency dependency of error vector

5.1.3 H field calculation

This section describes the measurement of the H field via the calibration coil, which is mounted at the bottom of the ISO tower. The conversion factor of the measured voltage by the oscilloscope probe to the H field strength is calculated in this section. This factor is significantly important for the calibration process of the test set-up. Furthermore, it is used for the H-field measurement of the EMVCo Setup, which is explained in chapter 5.2. Generally, the induced voltage in a coil is defined as:

$$U_i(t) = -N \frac{d\phi(t)}{dt} \quad (5.1.9)$$

$$\phi(t) = \int \vec{B}(t) \cdot d\vec{A}$$

$$\phi(t) = \int B(t) \, dA \cos(\alpha)$$

U_i is the induced voltage, N the number of windings of the coil and $\phi(t)$ the alternating magnetic flux.

The magnetic flux through a given surface is proportional to the number of magnetic B field lines that pass through the surface.

$$\phi(t) = \int \vec{B}(t) d\vec{A}$$

$$\phi(t) = \int B(t) dA \cos(\alpha)$$

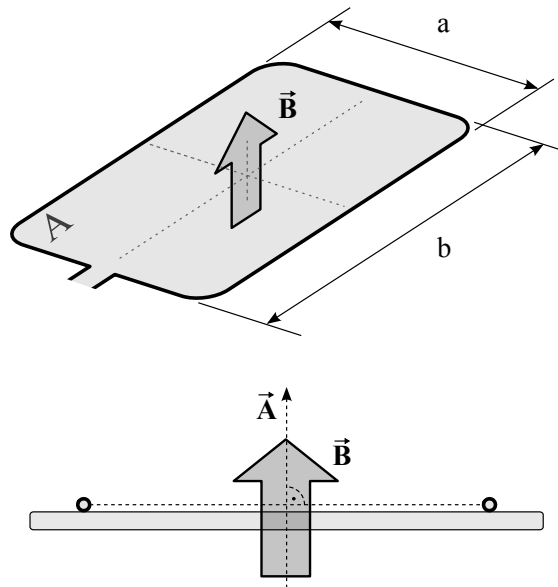


Figure 5.9: Card field geometry of calibration coil

Following conditions are presumed (figure 5.9):

- The surface area A is flat
- \vec{B} is the same all over the surface and proportional to

$$\vec{B}(t) \sim B \cos(\omega t)$$

- \vec{B} is perpendicular to the surface

$$\alpha = \angle(\vec{A}, \vec{B}) = 0$$

$\phi(t)$ can be written as

$$\begin{aligned}\phi(t) &= B A \cos(\omega t) \\ &= \mu_0 H A \cos(\omega t)\end{aligned}\quad (5.1.10)$$

H is the magnetic field strength and defined as:

$$\vec{H} = \mu_0 \mu_r \vec{B}$$

The area A of the surface is for simplicity:

$$\begin{aligned}A &= a \cdot b [m^2] \\ \vec{A} &= \vec{n} \cdot A\end{aligned}$$

Where \vec{n} is the normal vector of the surface. The evaluation of equation (5.1.9) yields the induced voltage:

$$\begin{aligned}U_i(t) &= -N \frac{d\phi(t)}{dt} \\ &= \underbrace{\mu_0 N A H \omega}_{u_i} \sin(\omega t)\end{aligned}$$

So a measured effective voltage U_{RMS} is related to H_{RMS} as

$$\begin{aligned}U_{RMS} &= \frac{1}{\sqrt{2}} u_i \\ &= \mu_0 N A \omega H_{RMS}\end{aligned}$$

and H_{RMS} can be calculated by evaluating

$$\begin{aligned}H_{RMS} &= \frac{1}{\underbrace{\mu_0 N A \omega}_{k_{RMS}}} U_{RMS} \\ &= k_{RMS} \cdot U_{RMS}\end{aligned}$$

From a measured Voltage $U_{pp} = \max(U_i(t)) - \min(U_i(t)) = 2u_i$ at the leads of the coil H_{RMS} is calculated as

$$\begin{aligned} H_{RMS} &= \frac{1}{\mu_0 N A \omega} \frac{U_{pp}}{2\sqrt{2}} \\ &= \frac{1}{\underbrace{2\sqrt{2} \mu_0 N A \omega}_{k_{pp}}} U_{pp} \\ &= k_{pp} \cdot U_{pp} \end{aligned}$$

Calibration Coil Parameters

$$a = 0.042 [m]$$

$$b = 0.072 [m]$$

$$\omega = 2\pi \cdot 13.56 \cdot 10^6 [Hz]$$

$$\mu_0 = 4\pi \cdot 10^{-7} [Vs A^{-1} m^{-1}]$$

$$N = 1$$

$$\begin{aligned} k_{RMS} &= \frac{1}{(4\pi \cdot 10^{-7}) \cdot 1 \cdot 0.003024 \cdot (2\pi \cdot 13.56 \cdot 10^6)} \\ &= \frac{1}{8\pi^2 \cdot 0.004100544} \\ &= 3.0887 A m^{-1} V^{-1} \end{aligned}$$

$$\begin{aligned} k_{pp} &= \frac{1}{2\sqrt{2} \cdot 4\pi \cdot 10^{-7} \cdot 1 \cdot 0.003024 \cdot 2\pi \cdot 13.56 \cdot 10^6} \\ &= 8\pi^2 \cdot 0.004100544 \cdot 2\sqrt{2} \\ &= 1.092 A m^{-1} V^{-1} \end{aligned}$$

5.2 EMVCo Set-up

EMV stands for *Europay International MasterCard VISA* and EMVCo is the organization of three companies which developed the payment standard for credit and debit cards. In contrast to the ISO set-up, the EMVCo set-up measures the impact of the load modulation on the reader's current and not any PICC parameters. Furthermore, the current i_1 through the reader antenna is calibrated to a constant value and is not swept as in the ISO set-up. The variation is done by changing the distance from the PICC to the PCD in defined slots. The EMVCo-tower is illustrated in figure 5.10 and looks like a multi level tower. At the bottom of the structure is the PCD antenna and the additional electrical circuit mounted. The z-direction, which passes from bottom to top, defines the distance from the PCD to the PICC. A change of the distance, according to the slots from zero to five, leads to a different mutual inductance $M(z)$. A electrical equivalent circuit for the system is shown in figure 5.11.

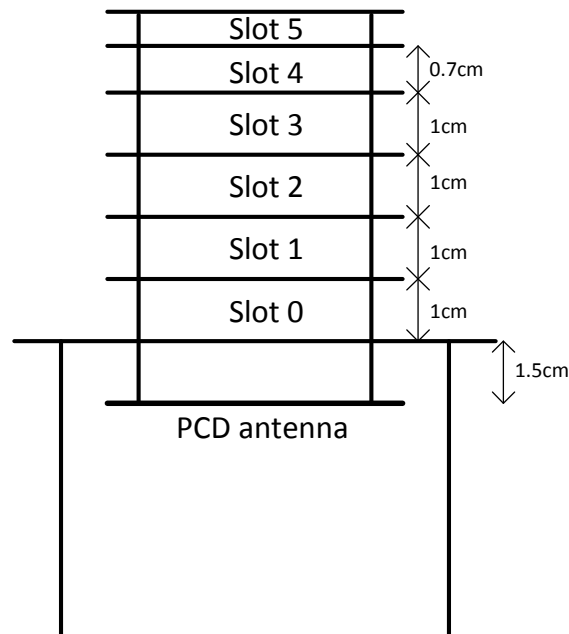


Figure 5.10: Front view of the EMVCo-Tower

It is important to say, that the EMVCo set-up contains a lot of different specifications and measurement descriptions. This master's thesis focuses on the load modulation of the PICC and the results to the PCD.

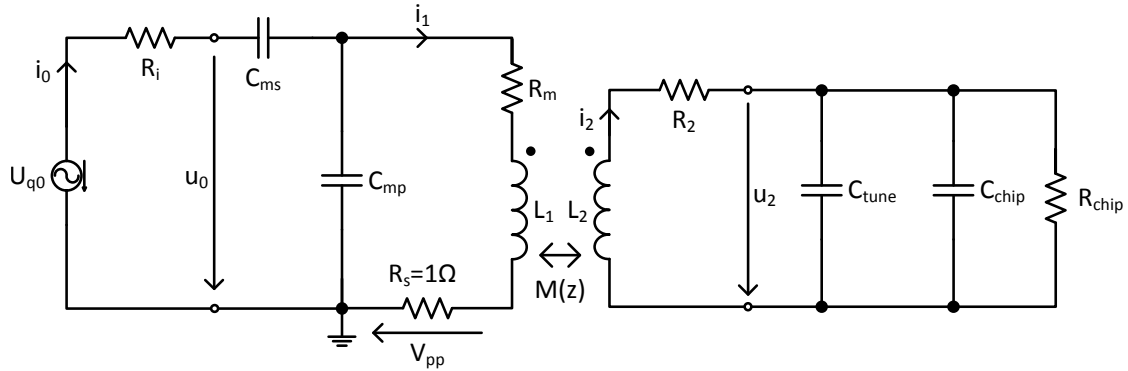


Figure 5.11: Equivalent circuit for EMVCo Set-up

Part	Value
L_{PCD}	614 nH
R_{Li}	0.58 Ω
R_i	50 Ω
R_s	1 Ω
R_m	0.375 Ω
$Q = \frac{wL}{R}$	27.9

Table 5.2: Values for EMVCo PCD

The voltage V_{pp} is measured by the EMVCo measurement board during load modulation of the PICC. As the shunt resistors value R_s is 1 Ω , the measured voltage is equal to the antenna current i_1 . Generally, the EMVCo measurement board uses a special subcarrier demodulator for the demodulation of the modulated signal, which is kept secret by the company. The quality factor Q of the PCD antenna (with a compensation winding) lies between 15 and 20 and can be regulated by the additional serial resistor R_m , which's value should be between 0.5 and 1 Ω .

The measured values for the EMVCo PCD are shown in table 5.2.

Following field strengths were measured by a calibration coil at the slots of the calibrated EMVCo tower according to the standard Paypass-ISO/IEC 14443 [10], which describes the requirements and measurement instructions for contactless payment.

Typically, the modulated signal is very small compared to the quiescent current in the PCD antenna. Figure 5.12 illustrates the current i_1 , respectively the voltage V_{pp} at load modulation. The signal consists of an alternating 0 and 1 bit stream, which must be

Slot number	coupling factor k	mutual inductance M
Slot 0:	0.1187	8.1145e-8
Slot 1:	0.0786	3.3866e-8
Slot 2:	0.0507	2.1835e-8
Slot 3:	0.0341	1.4692e-8
Slot 4:	0.0239	1.0312e-8
Slot 5:	0.0185	7.9679e-8

Table 5.3: Coupling factors and mutual inductances of PCD and PICC (4 coil turns, ID1)

Slot number	$U_{induced}$ in Vpp	Field Strength in A/m (= $1.1 \times U_{induced}$)
Slot 0:	7.87	8.657
Slot 1:	4.93	5.423
Slot 2:	3.29	3.619
Slot 3:	2.22	2.442
Slot 4:	1.6	1.76
Slot 5:	1.29	1.419

Table 5.4: Measured field strength at slots with calibration coil

present for the measurement of load modulation. After the demodulation of the signal in figure 5.12, the load modulation voltage V_{pp} can be determined (illustrated in figure 5.13). Generally, the measured V_{pp} values per bit are averaged over the acquired signal length. Although the modulated current i_2 is a rectangular signal, the demodulated signal looks like a sawtooth because the coupled system acts like a filter. The higher the quality factor of the system, the higher is the filter level.

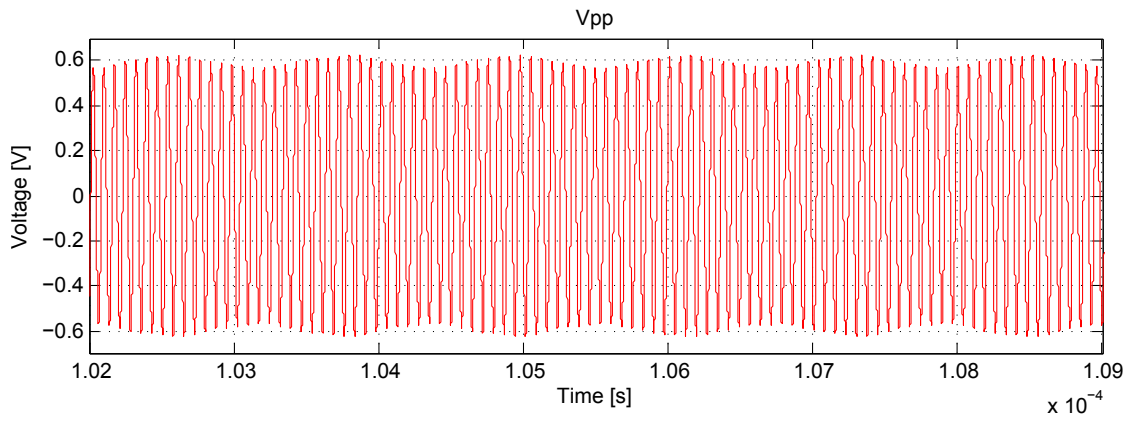


Figure 5.12: PCD current i_1 at load modulation

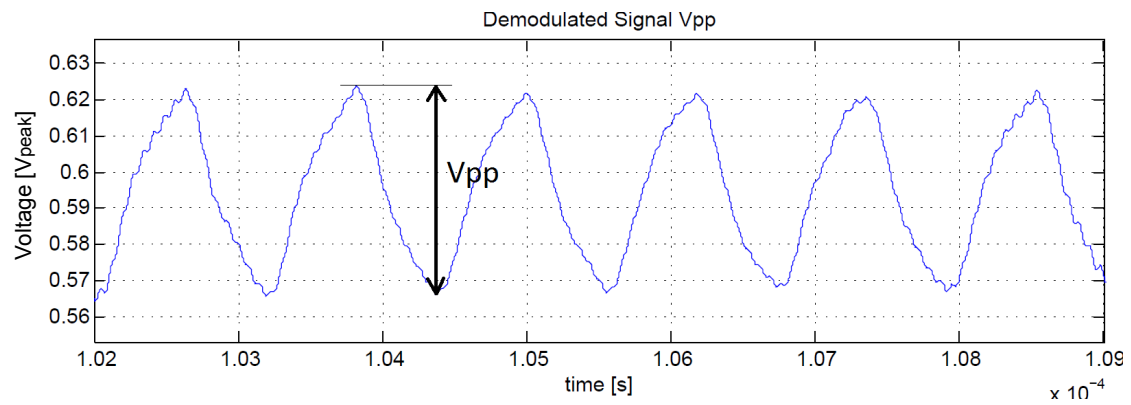


Figure 5.13: Demodulated signal and definition of V_{pp}

Chapter 6: LM Analysis Tool

This chapter explains the structure, functionality and implementation of the analysis tool for load modulation. The *Load Modulation Analysis Tool* is programmed in Matlab, the abbreviation for MATrix LABoratory. This programming language is optimized for calculations of numeric problems, data acquisition, data analysis and for the visualization of data. That's why this programming language was optimal and therefore used for the implementation of the analysis tool.

Basically, this program is optimized for the analysis of load modulation by the ISO set-up. Nevertheless, it is able to analyze the acquired data by an EMVCo set-up and an ADS simulation.

6.1 Measuring and Analysis Process

6.1.1 General Steps

Following general steps need to be pursued for the analysis of load modulation with the ISO set-up:

1. Data Acquisition
 - Tune the PICC to a specific resonance frequency
 - Put the PICC on the ISO tower
 - Measure signals with PIXIE measurement tool (LabVIEW tool of Infineon)
 - Calibrate the ISO set-up (error vector, field strength)
 - Define oscilloscope settings (trigger, time delay, duration)
 - Download a request command to the function generator for the correct type (type A or B)

- Define field strength sweep (start, stop, step size)
- Run automated data recording (save data in CSV format)
- Sort data to correct folder structure (see 6.3.1)
- Repeat process of measuring without PICC for error vector recording

2. Data Analysis

- Start Matlab analysis tool
- Set options and links to data folders (modulated signal, error signal)
- Start associated analysis
- Data will be analyzed, displayed and saved

6.1.2 Measuring Arrangement

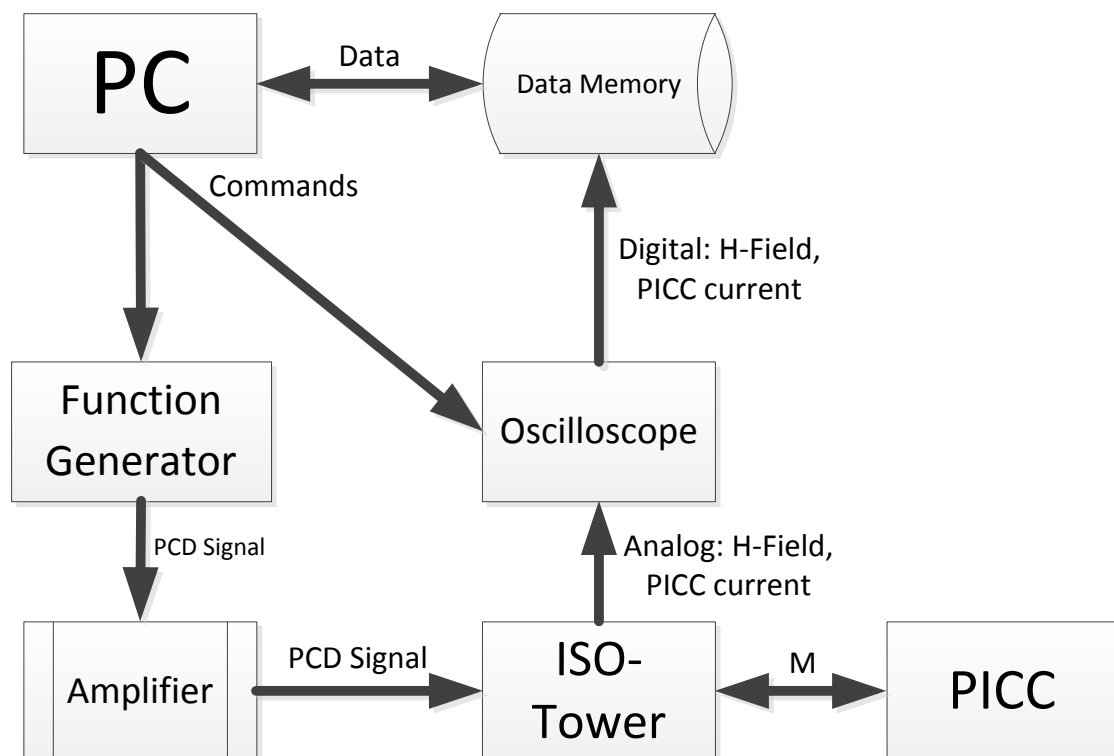


Figure 6.1: ISO-Measuring arrangement

Figure 6.1 shows the measurement structure with its components and connections. The measuring process is controlled by the user via the PC. Fundamentally, the user is able to define a sequential sequence of instructions by the *LabVIEW* tool *PIXIE*. Afterwards, the software executes the instructions automatically. Firstly, the set-up is calibrated according to the field strength sweep options. The function generator sends an AC voltage sweep to the amplifier which amplifies the signal by a nearly constant factor. The output of the amplifier is directly connected to the PCD (ISO tower) and therefore a magnetic field is generated. Typically, the field strength is measured by the calibration coil at the bottom stage of the ISO tower. So the PC is able to check the relation between the sent and received voltage for field strength calibration. After this calibration process, the PC sends a request command to the function generator, which is needed for starting the communication with the PICC. Otherwise, there would not occur any load modulation through the PICC because it would remain in an idle mode. The command is saved by the function generator and is used for every field strength point. Next, a loop iteration starts according to the defined field strength range. It can be defined by a start point, an end point and the step size between two points. Principally, the loop iteration starts at the smallest or biggest field strength point and passes iteratively to its defined point at the opposite. During the sweep, the PC saves the digitalized signals by the oscilloscope for every field strength point to the data memory. It is important to say, that the oscilloscope has to be correctly set to the load modulation signal through the trigger and timing options. According to ISO, the signal must contain exactly six subcarrier cycles of the modulated signal and the modulated signal must be an alternating combination of zeros and ones. For the evaluation by the analysis tool, typically, eight cycles are recorded because the used filter mechanism has a settling time and therefore, the first and last cycles are removed. Dependent on the field strength sweep, several hundred mega bytes of data can be accumulated.

The PC communicates with the function generator and oscilloscope via a GPIB (General Purpose Interface Bus) interface. Generally, the function generator is connected by a coaxial BNC (Bayonet Nut Connector) cable to the amplifier, which is needed, because the output power of the function generator is too low. Next, the signal is carried on from the amplifier to the ISO-tower with an SMA cable. Furthermore, it must be noted that channel one and three or channel two and four should be used for data acquisition, if a four-channel oscilloscope is used. The reason for this is that the sampling rate can be doubled and the saved sampling time of the two channel corresponds more exactly.

6.2 Data Analysis

This section describes the purchased results of the LM analysis tool. Basically, the information is calculated for every measured chip and is visualized in comparison to each other in one figure for a field strength or resonance frequency point. The x axis of the figures is either the swept field strength or the resonance frequency. Furthermore, the displayed waveforms are drawn in separated colours to obtain a clear distinction of the chips. In addition, dashed lines are used to visualize a second result parameter in a figure. Following points are determined out of the accumulated data in the subsequent subsections.

6.2.1 Voltage Load Modulation Amplitude

Generally, the VLMA is determined for every given field strength point. The explanation for VLMA is given in section 5.1.1.

6.2.2 Amplitude Difference

amplitude difference is defined as the difference of the amplitude levels from the high and low state of the modulated subcarrier signal in the PICC (in Volt peak). High and low state values are measured at the stable states of the demodulated signal. Additionally, an averaging is done over all subcarrier cycles.



Figure 6.2: Amplitude difference of modulated current

6.2.3 Phase Difference

The phase difference is defined as the absolute phase difference of the high and low state of the demodulated subcarrier signal. Principally, high and low state values are measured at the stable states of the rectangular signal as shown in figure 6.3. Additionally, an averaging is done over all subcarrier cycles.

The phase of the signal is referenced to the recorded field strength signal, which is nearly constant at load modulation. In addition, it should be noted that the phase of the induced voltage in the calibration coil (field strength measurement) has the same phase position as the induced voltage in the PICC.

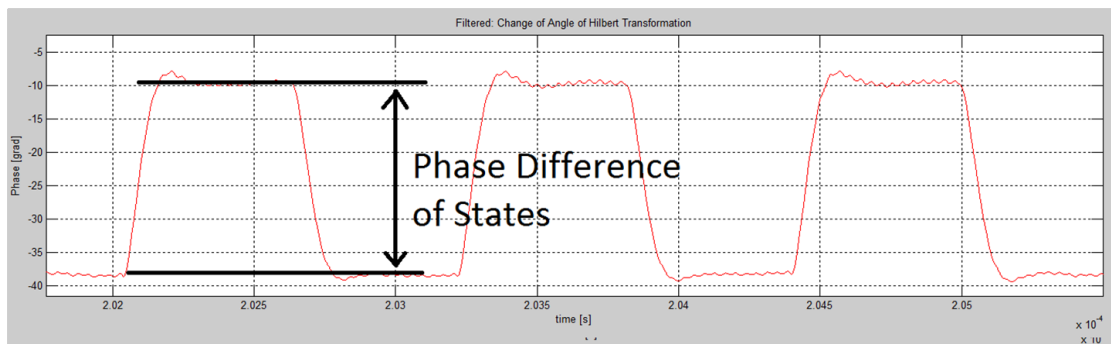


Figure 6.3: Phase difference of modulated current

6.2.4 Amplitude of Difference Vector

According to the determination of the amplitude and phase position of the modulated and unmodulated state, the states can be represented as vectors (illustrated in figure 6.4). The difference vector lies between these two vector states and gives information about the efficiency of load modulation. The higher the amplitude of the difference vector, the higher is the efficiency of the modulation and the smaller is the possibility for the transmission of bit errors.

6.2.5 Pointer Diagram of Signal

The pointer diagram of the signal states gives an overview over a large amount of information (figure 6.4). In simplified terms, this means that the pointer diagram

provides information about the amplitude and phase states for every field strength point. If the imaginary part of the current pointer is positive, the impedance of the PICC is capacitive because the current runs forward related to the induced voltage. Vice versa, the PICC impedance is inductive, if the imaginary part of the current is negative. It is important to say, that the length of the current vectors are not equal to the magnitude of the current i_2 , because the measured bridge voltage can not be mapped by one to one.

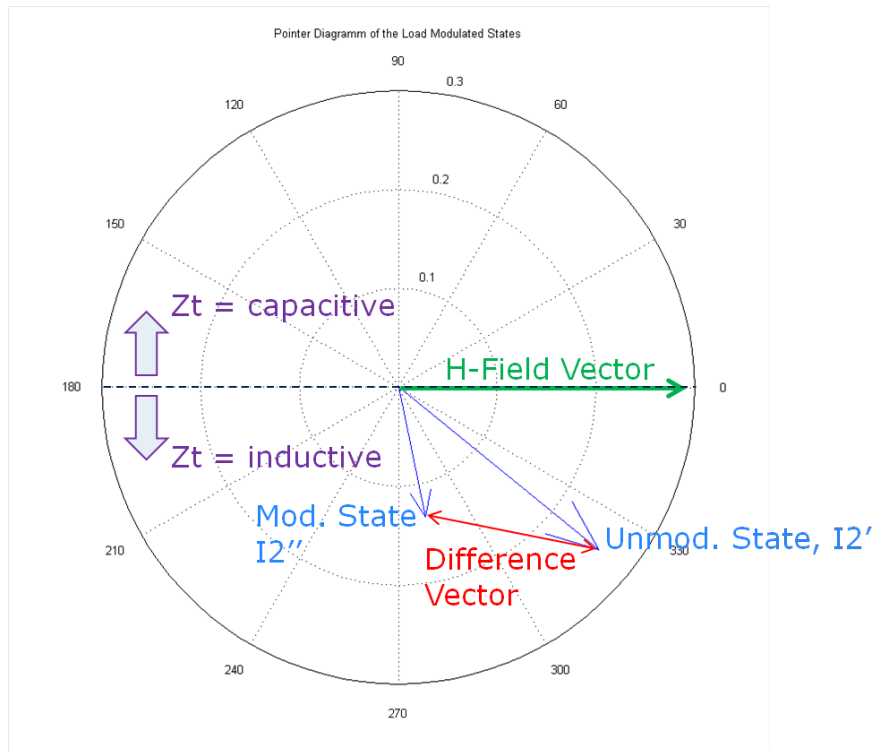


Figure 6.4: Pointer diagram of signal states

6.2.6 Overshoot/Undershoot and Rise/Fall Time of Amplitude and Phase

Figure 6.5 illustrates the definition of overshoot, undershoot, rise and fall time according to a rectangular waveform. They result from the extremely alternating quality factor of the resonance circuit related to load modulation. As the system is dynamically, the alternating signal needs a certain time to reach the new stable current state related to the resonance circuit. The larger the change of the quality factor, the greater is the overshoot, undershoot, rise and fall time. An optimal behavior would be the smallest

possible overshoot, undershoot, rise and fall time of the current i_2 .

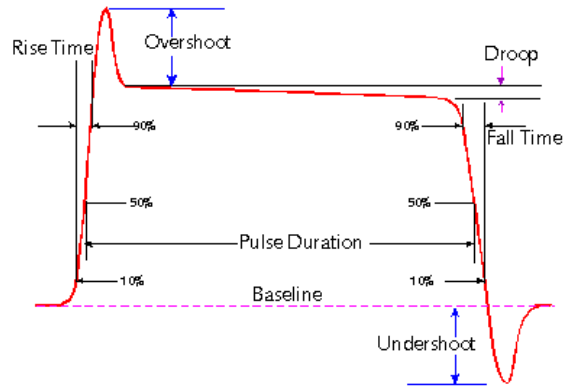


Figure 6.5: Waveform parameters (adapted from [1])

6.2.7 Equivalent Circuit

Figure 6.6 illustrates the equivalent circuit for the PICC. Generally we can summarize:

- **Known component values:**
 - Antenna inductance L_2
 - Internal resistance of antenna R_2
 - Tuning capacity C_{tune}
- **Measured signals:**
 - Antenna current i_2
 - Induced voltage U_{q2}
- **Following parts can be calculated:**
 - Load resistor R_L
 - Chip capacity C_{chip}
 - Chip supply voltage U_2
 - Chip resonance frequency f_{res}
 - PICC impedance \underline{Z}_T

The antenna characteristics can be measured with an impedance analyzer and are typically for a 4 coil turn ID-1 card: $L_2 = 2.3 \mu H$ and $R_2 = 1.8 \Omega$. The external tuning capacity C_{tune} is typically also known and dependent on the resonance frequency adjustment. As mentioned before, the ISO-Setup gives information about the antenna current i_2 and the induced voltage U_{q2} . It is important to say, that these values have to be scaled by a factor. Additionally, the current i_2 has to be phase corrected mathematically.

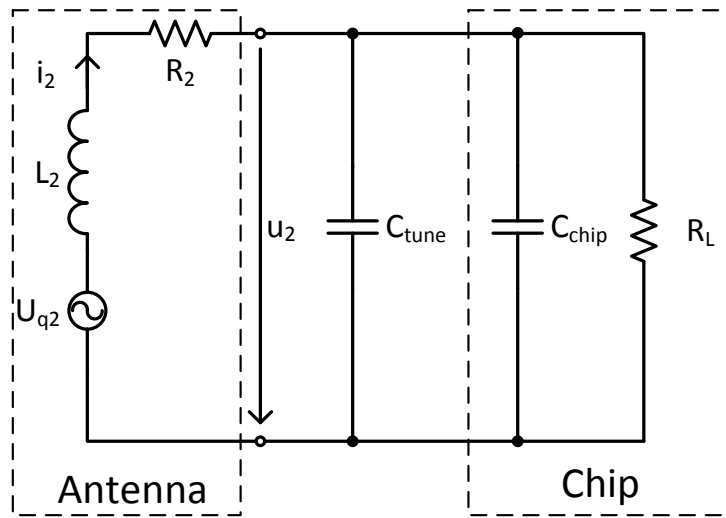


Figure 6.6: PICC equivalent circuit for calculation

Relation between measured voltage by calibration coil and induced voltage U_{q2} :

$$\underline{U}_{induced} = j\omega M \cdot i_1 \quad (6.2.1)$$

$$M = k \cdot \sqrt{L_a L_b} \quad (6.2.2)$$

$$k_U = \frac{U_{q2}}{U_{cal}} = \frac{j\omega M_{pcd,picc} \cdot i_1}{j\omega M_{pcd,cal} \cdot i_1} = \frac{\sqrt{L_{pcd} L_{picc}}}{\sqrt{L_{pcd} L_{cal}}} \quad (6.2.3)$$

Calculation for values according to table 5.1:

$$k_U = \frac{\sqrt{495 \cdot 10^{-9} \cdot 2.3 \cdot 10^{-6}}}{\sqrt{495 \cdot 10^{-9} \cdot 230 \cdot 10^{-9}}} = 3.16228 \quad (6.2.4)$$

Relation between measured voltage by bridge and PICC antenna current i_2 :

As mentioned in section 5.1.2, there exists an error vector because of geometrical inaccuracies and production tolerances of the ISO-tower. Investigations have shown, that the error vector can be mathematically subtracted from the acquired signal to get the correct signal. This is only successful, when the error vector results of different coupling factors to the sense coils. Additionally, every error vector has to be known for each field strength point and the compensation has to be done for every point.

The first plot in figure 6.7 shows the magnitude of the error vector for different coupling factors. If Δk is zero, the measuring bridge is ideal and the magnitude of the error vector is zero. The second plot illustrates the angle of the error vector, which is constant for the coupling factor sweep. Moreover, the third and fourth plot in the figure illustrate the correction factor without the compensation of the error vector, which is needed for the correct calculation of i_2 . Basically, the correction factor is not constant for different coupling factors and therefore a fault is generated. The fifth plot in figure 6.7 represents the magnitude and the sixth plot the angle of the correction factor. It is important to say, that the error vector is already subtracted from the measured signal. As a result, the correction factor is constant over the whole coupling factor sweep, which means that a correct compensation is possible. The potentiometer of the measuring bridge is kept constant over the hole sweep.

Figure 6.8 illustrates the error voltage, the correction factor without noise compensation and the correction factor with noise compensation. As shown in the last two plots, the correction factor is not constant for different sense coil inductances, although the error vector was subtracted from the signal (= noise compensation). If the inductance value L_A equals L_B , the magnitude of the correction factor is 6.203 and the phase 82.75 degree. The values are calculated for a constant potentiometer value at the bridge, which means that the failure can be minimized by adjusting the potentiometer, but nevertheless, it can not be fully eliminated.

In practice the error voltage is typically smaller than 50 mV at a field strength of 1.5 A/m.

An experiment has shown, that the subtraction of the acquired error signal from the measurement bridge signal leads to pretty good results. Figure 6.9 illustrates the experiment. The signal of a serial resonance circuit was acquired by two different ISO-towers.

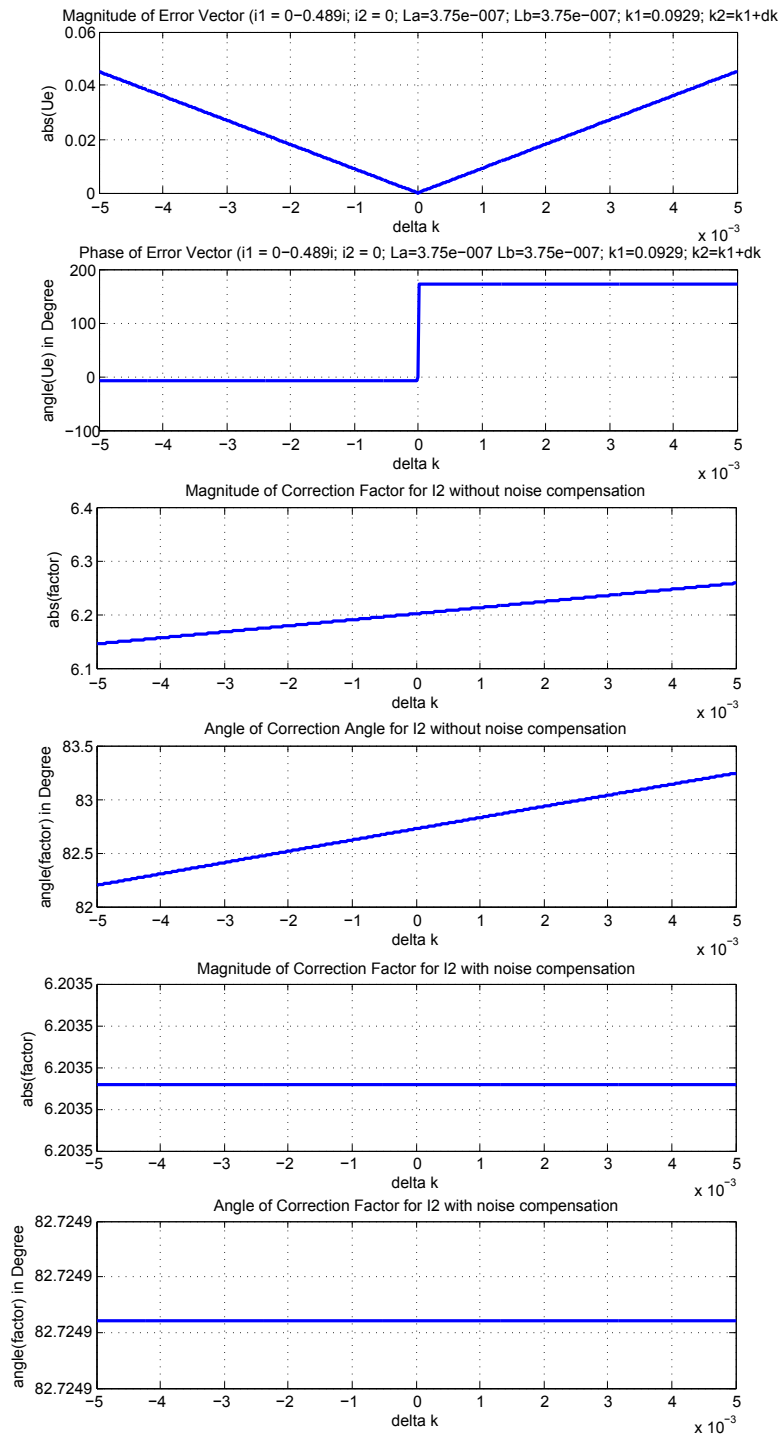


Figure 6.7: Correction factor for i_2 without and with error compensation for different coupling factors

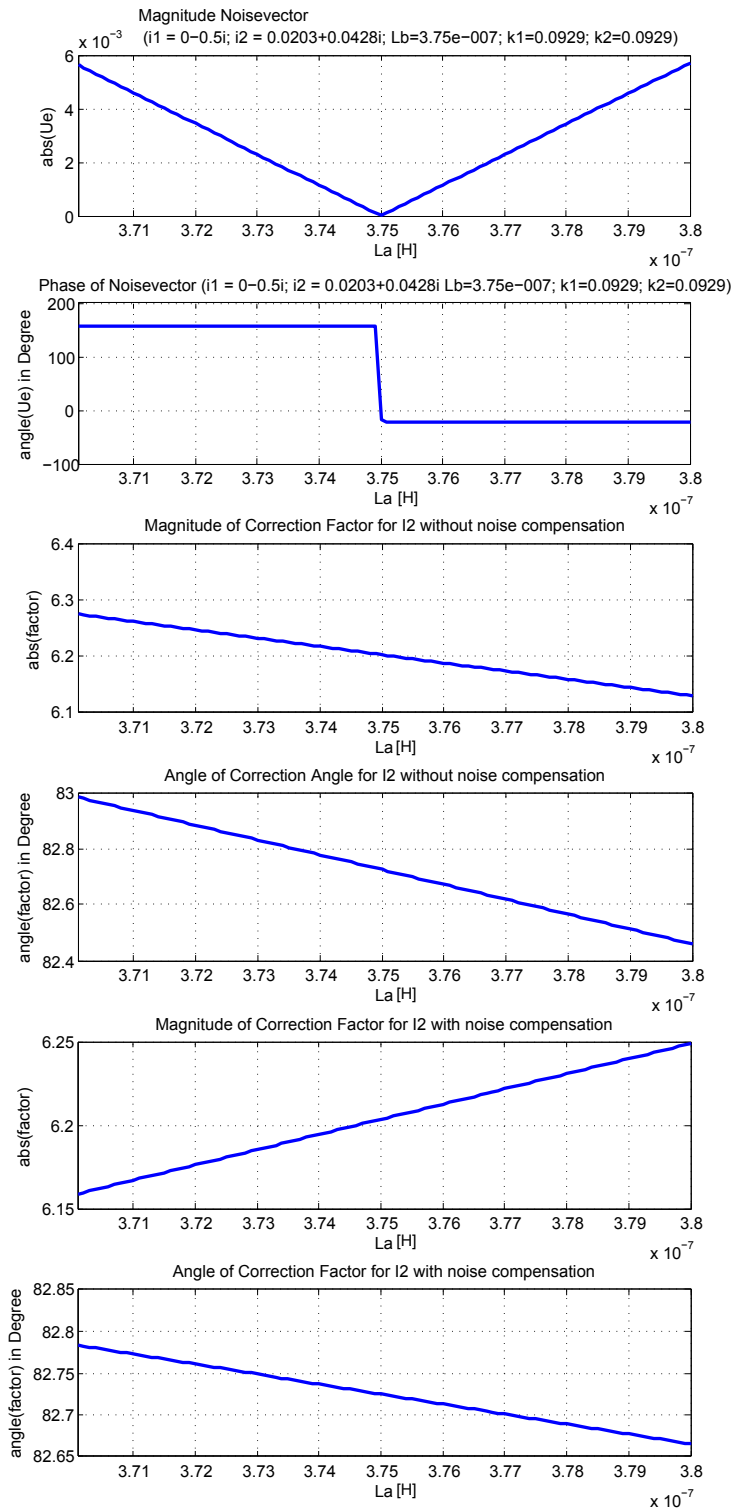


Figure 6.8: Correction factor for i_2 without and with error compensation for different sense coil values

As shown in the first plot of the figure, the noise vector of tower 13 is twice higher than the error vector of tower 5. Furthermore, the length of the vectors are not equal and the phase is shifted. The second plot in the figure illustrates the signal after the subtraction of the noise signal (= error vector). The compensation process leads to equal vectors according to their magnitude and phase, although the ISO-towers differ in their characteristics. The 180 degree shift between the two vectors occurs of interchanged sense coil connections at the two ISO-towers. In response to this successful experiment, the compensation process should be done for every analysis process. Investigations have shown, that the error vector can shift the real signal by up to 20 degrees! This means that especially the calculation of the equivalent circuit for the PICC would lead to big divergences.

The correction of the acquired signals U_{cal} and u_d leads to the PICC antenna current i_2 and the induced voltage U_{q2} . Remaining unknown values for the equivalent circuit can be calculated through the picked up signals as shown in formula 6.2.5 to 6.2.13.

$$\underline{u}_d(wt) = A_d \cdot e^{j(wt+\varphi_d)} \quad (6.2.5)$$

$$\underline{i}_2(wt) = \frac{A_d}{|\text{correction factor}|} \cdot e^{j(wt+\varphi_d+\angle\text{correctionFactor})} = \frac{A_d}{6.203} \cdot e^{j(wt+\varphi_d+82.75^\circ)} \quad (6.2.6)$$

$$\underline{I}_2 = \hat{i}_2 \cdot (\cos(\varphi_d + \angle\text{correctionFactor}) + j \cdot \sin(\varphi_d + \angle\text{correctionFactor})) \quad (6.2.7)$$

$$\underline{U}_{q2} = \underline{U}_{cal} \cdot k_U = \underline{U}_{cal} \cdot 3.16228 \quad (6.2.8)$$

$$\underline{Z}_{PICC} = \frac{U_{q2}}{I_2} = \Re\{\underline{Z}_{PICC}\} + \Im\{\underline{Z}_{PICC}\} = jwL_2 + R_2 + \frac{R_L - jwC_2R_L^2}{1 + R_L^2w^2C_2^2} \quad (6.2.9)$$

$$\Rightarrow R_L = -\frac{L_2^2w^2 - 2wL_2\Im\{\underline{Z}_{PICC}\} + R_2^2 - 2R_2\Re\{\underline{Z}_{PICC}\} + \Im\{\underline{Z}_{PICC}\}^2 + \Re\{\underline{Z}_{PICC}\}^2}{R_2 - \Re\{\underline{Z}_{PICC}\}} \quad (6.2.10)$$

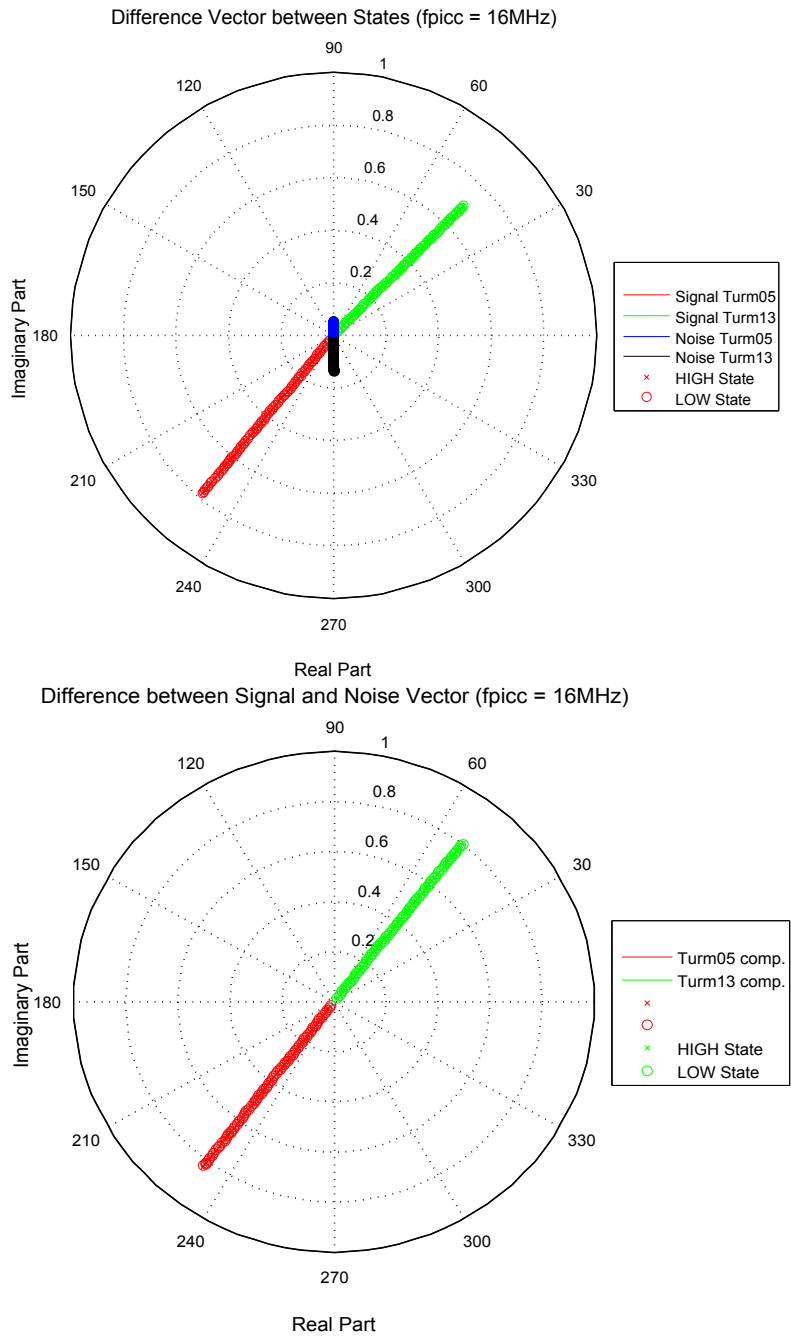


Figure 6.9: Experiment: Noise vector compensation

$$\Rightarrow C_2 = \frac{\sqrt{(R_2 + R_L - \Re\{Z_{PICC}\})}}{\Re\{Z_{PICC}\}w^2R_L^2 - R_2w^2R_L^2} \quad (6.2.11)$$

$$U_2 = \left| I_2 \cdot \frac{R_L - jwC_2R_L^2}{1 + R_L^2w^2C_2^2} \right| \quad (6.2.12)$$

$$f_{res} = \frac{\sqrt{\frac{1}{C_2L_2} - \frac{1}{R_L^2C_2^2}}}{2\pi} \quad (6.2.13)$$

6.2.8 EMVCo Vpp Estimation

The EMVCo set-up is explained in section 5.2 and its focus lies on the observation of the PCD current. This set-up is in practice quite unpopular and time-consuming because the measurement has to be done manually by sticking the PICC in every slot. As described in the last section, the impedance of the PICC can be mathematically calculated. The transformed transponder impedance for the PCD can be calculated with the formulas in section 4.3 and values in table 5.2, 5.3 and 5.4. The field strength values in table 5.4 for EMVCo set-up can be matched to the ISO set-up. The behavior of the PICC is dependent on the field strength and therefore a relation between the two measurement systems can be established. As a result, the PICC impedance can be measured and calculated with the ISO set-up for the given field strength points and formula 4.3.1 can be used for calculation of the effect to the EMVCo reader current i_1 . In this way, it is possible to make a quite good prediction for the load modulation value V_{pp} of the EMVCo set-up by the measurement through the ISO set-up. The big advantage is that the Chip can be checked in parallel for both standards with the ISO set-up, which is an automated process.

6.3 Program Structure and Functions

Figure 6.1 illustrates the functions of the Matlab program and their calling hierarchy. As the tool is programmed like a script, the data flow is straight forward and has no dependency between the functions of a hierarchy level. The following subsections explain the functions of the tools with their parameters and general tasks.

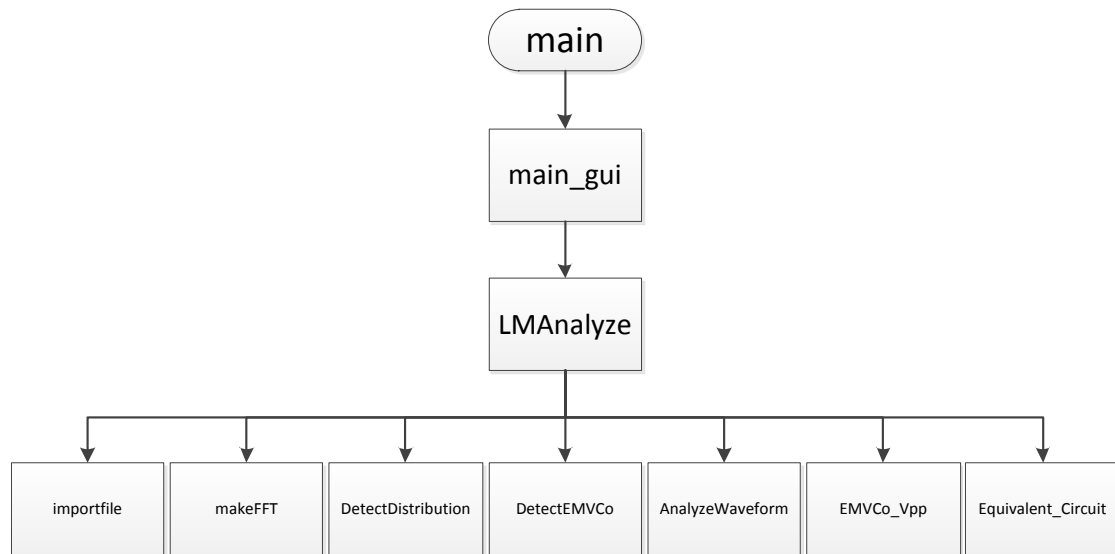


Figure 6.10: Program functions and calling structure

6.3.1 Main GUI

This program interacts with the user by a graphical user interface (GUI), as shown in figure 6.11. It is important to say, that the number of field strength points and resonance frequencies has to be equal for every measured chip for *Multiple Analysis!*

GUI Description (figure 6.11):

1. **Single Analysis:** On the left side of the GUI is the option for a single analysis of a specific field strength point. The analyzed results will be displayed at the boxes after the single analysis has finished.
2. **Plot Options:** The user has the possibility to define the figures, which should be plotted for every point. Typically, all points are disabled for the multiple analysis type because otherwise it would lead to too many figures.
3. **ISO VLMA calculator:** The minimal VLMA value according to ISO standard can be calculated for a specific field strength.
4. **Multiple Analysis:** This option is for the analysis of one or more chips. The field strength sweep and the resonance frequencies for the acquired data need to be defined. The link to the data folder has to be set at the top of the panel.

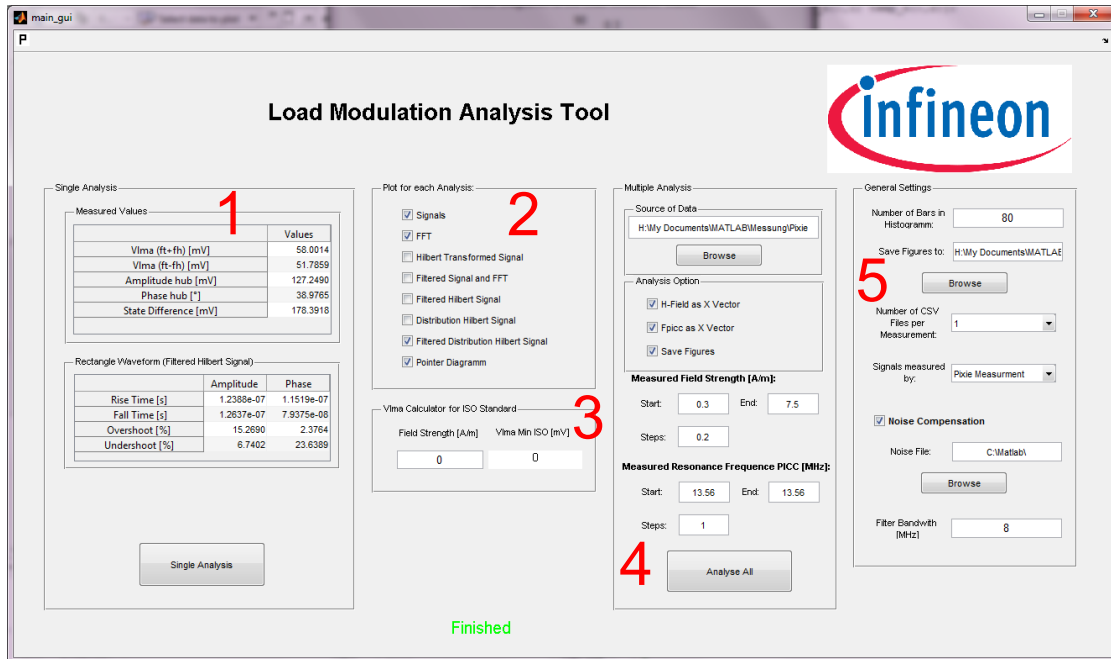


Figure 6.11: Graphical User Interface

The user has the possibility to choose in the *Analysis Option* panel, if the figures shall be saved and if the data shall be plotted over the field strength and PICC resonance frequency. *General Settings* panel consists of options for *Single Analysis* and *Multiple Analysis*. *Number of Bars in Histogram* defines the resolution of the analysis for the amplitude range of the signal. The next field defines the folder where the figures are saved to automatically. Then there follow two drop boxes where the type of measurement and the number of saved files per field strength point need to be defined. Next, the option for noise compensation and the associated data folder can be set. Last but not least, the filter bandwidth of the IIR filter needs to be defined, which is used to suppress the white noise of the analog signal.

Defined data structure for data storage:

Following data structure for *Multiple Analysis* must be kept:

- main folder (eg.: Measurement-2011-11)
 - sub folders: Chip names (eg.: Chip1, Chip2, Chip3)

- * sub sub folders: Resonance frequencies (eg.: 13MHz, 15MHz, 17MHz)
- in sub sub folders: Data Files of field strength sweep (eg.: Chip1-1Am.csv, Chip1-2Am.csv, Chip1-3Am.csv)

6.3.2 Function LMAnalyze

Passing parameters:

- Plot option for figures: 0 for disable, 1 for enable
- Number of bars for histogram amplitude analysis
- Directory paths to data and noise signals
- Measurement type
- Filter bandwidth

Return parameters:

- Amplitude and phase difference
- VLMA of upper and lower sideband
- Vectors of states
- Parameters of rectangular waveform (overshoot, undershoot, rise and fall time) for amplitude and phase
- EMVCo Vpp load modulation prediction
- PICC impedance
- Calculated parameters: $I_1, R_L, C_2, f_{res}, U_2$

Description:

The main task of the function *LMAnalyze(...)* is the analysis of load modulation for one measured signal pair. This signal pair consists of the bridge voltage ($\propto i_2$) and the field strength voltage ($\propto U_{q2}$). First of all, it calls the function *importfile(...)* for data loading. Secondly, the function subtracts the noise signal from the bridge signal if *noise compensation* is activated. Thirdly, the function *makeFFT(...)* is called for VLMA determination. Then, the measured signal pair is filtered with an IIR filter with the entered bandwidth. This filter has an order of eight and is defined as a Butterworth filter. The analytical signal of the signal pair is calculated through the

Hilbert transformation. Furthermore, the function *DetectDistribution(...)* is called, which detects the stable states of the amplitude and phase signal. It analysis the relation between the phase and amplitude to determine the two state vectors. Then *AnalyzeWaveform(...)* determines the overshoot, undershoot, rise and fall time of the signals. Afterwards, the function *EMVCo_Vpp(...)* calculates the estimation for EMVCo set-up and the function *Equivalent_Circuit(...)* computes the parameters for the equivalent circuit of the PICC. During this procedure, the desired figures according to the *Plot Options* are plotted.

6.3.3 Function importfile

Passing parameters:

- Channel or Path: current (1), magnetic field (2), noise vector (3)
- Path and Data format extension: .csv or .txt
- Delimiter of data values: comma or tabulator
- Number of headlines in data file

Return parameters:

- Data structure of signal(s)

Description:

This function imports the stored data from the hard disc into a variable, which has a structured format. If a path is set through the first passing parameter, no extra window for the selection of a folder is popped up. Otherwise, the user has to select every channel file manually in the single analysis mode.

6.3.4 Function makeFFT

Passing parameters:

- Signal in matrix form: first column is time vector, second column is amplitude vector
- Plot option for spectrum: 0 deactivated, 1 activated

Return parameters:

- VLMA value for upper and lower sideband
- Magnitude of carrier signal

Description:

The passing signal must contain exactly six cycles of the subcarrier signal with 847.5 kHz. Furthermore, it must be an alternating bit stream of zero's and one's and therefore two consecutive bits are not allowed. First of all, the signal is windowed with a Bartlett window, which is prescribed in the ISO standard. This is done to suppress the leakage effect, which creates undesired frequency components. The leakage effect is a phenomenon in the signal analysis, which occurs when a time-limited signal is analyzed in its frequency domain. In the next step, the signal is zero padded to a desired length. The reason for this is that the DFT has discrete scan points in the frequency spectrum and the scan points should lie exactly at the carrier and subcarrier frequencies. This guarantees the correct measurement of VLMA. Afterwards, the DFT (Discrete Fourier Transform) is calculated and the magnitude of the amplitude spectrum is measured at the desired scan points f_c , $f_c - f_m$ and $f_c + f_m$ (illustrated in figure 5.1).

The frequency spectrum can be plotted as a single sided spectrum and a double sided spectrum.

6.3.5 Function DetectDistribution

Passing parameters:

- Histogram of signal amplitude: Number of bars, amplitude range

Return parameters:

- Mean value of high and low state in Volt peak
- Difference between states

Description:

This function detects the stable states of the modulated signal. The passing parameters are the histogram parameters of the analytical signal. The analytical signal and its histogram distribution are shown in figure 6.12. Furthermore, the values of the detected states and the state difference are displayed in the last two plots. The states are detected

with a Gaussian fitting algorithm. This algorithm fits the histogram distribution with a Gaussian curve because the signal is overlaid with a white noise and its deviation has a Gaussian form. The stable state equals the mean value of the fitted Gaussian curve, which is shown in figure 6.13. The difference of the stable states is therefore then the difference between the detected mean values.

6.3.6 Function DetectEMVCo

Passing parameters:

- Signal in matrix form: first column is time vector, second column is amplitude vector

Return parameters:

- Load modulation Vpp states
- Load modulation voltage Vpp (difference between states)

Description:

This function is used, when the analysis shall be done for EMVCo set-up. It works similar to the function *DetectDistribution(...)* but in contrast to it, the function detects the states not with a Gaussian fitting algorithm but with a maximum and minimum detection over every period. Additionally, the detected maxima and minima are averaged over all periods.

6.3.7 Function AnalyzeWaveform

Passing parameters:

- Amplitude vector of signal
- Time vector of signal
- Detected high and low state of modulated signal

Return parameters:

- Overshoot and undershoot of modulated signal
- Rise and fall time of modulated signal

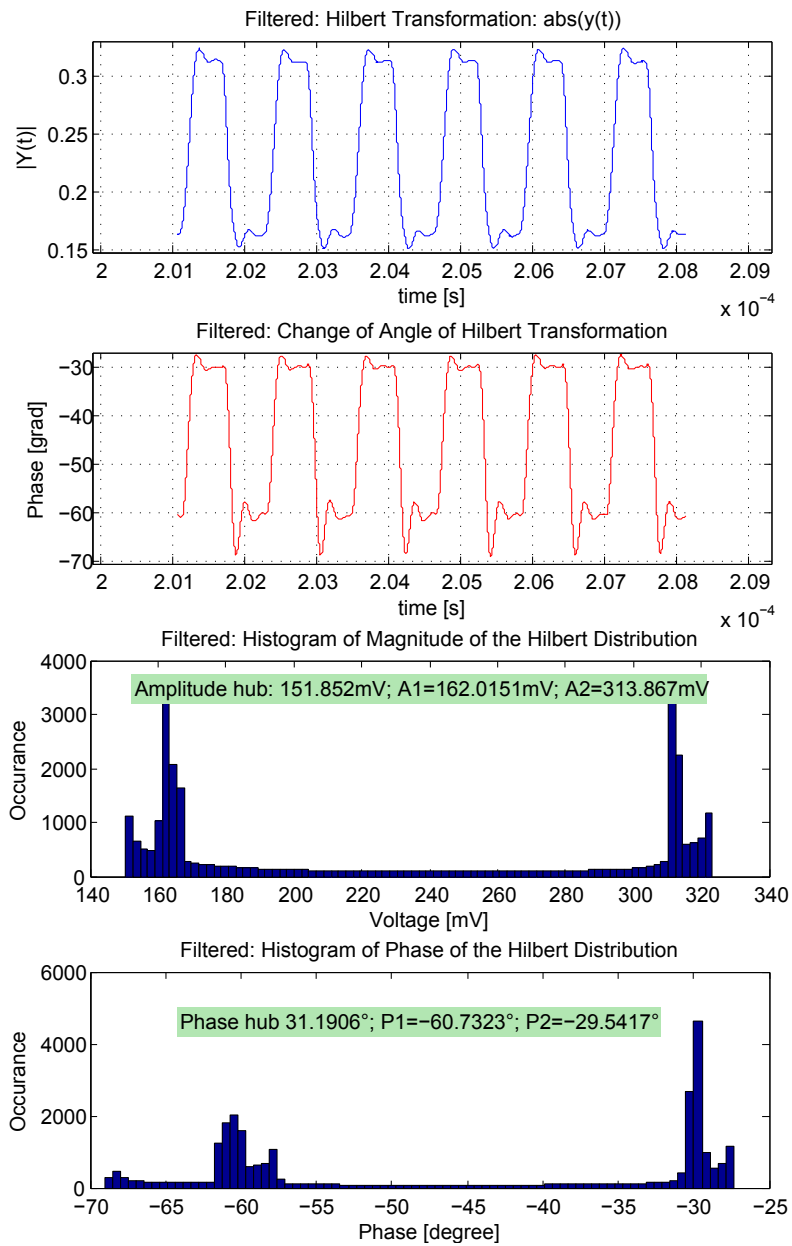


Figure 6.12: Detection of distribution via histogram analysis

Description:

This function analyzes the rectangular waveforms of the six subcarrier cycles according to figure 6.5. An algorithm detects the null walk through for every period and searches the 10 and 90 percent levels of the signal for time measurement. Via the maximum and

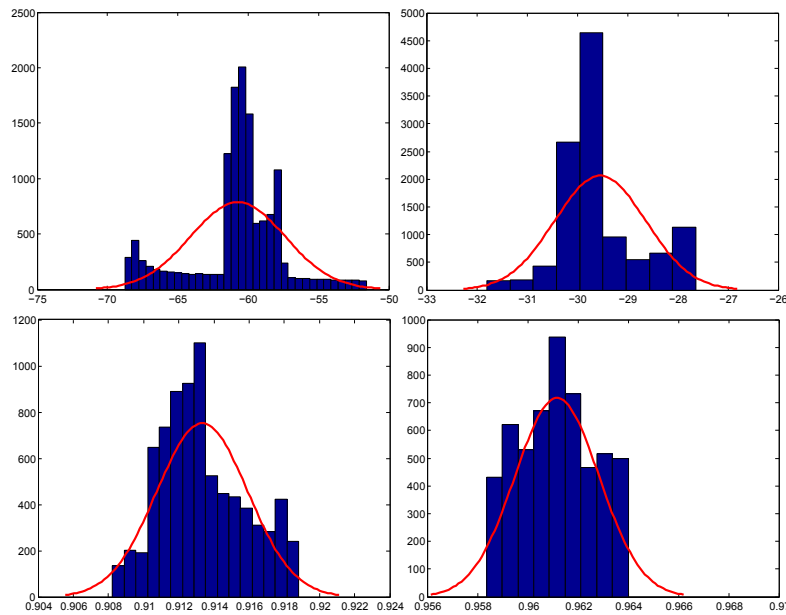


Figure 6.13: Gaussian fitting algorithm for state detection

minimum level detection and the stable high and low level of the period, the overshoot and undershoot can be calculated. Finally, the determined values are averaged over all subcarrier periods.

6.3.8 Function Equivalent Circuit

Passing parameters:

- Vector states of current \underline{I}_2
- Voltage states of calibration coil U_d

Return parameters:

- Parallel resistor and capacity of equivalent circuit (R_L, C_p)
- Resonance frequency f_{res} of PICC
- Supply Voltage U_2 of Chip in V_{DC}

Description:

This function calculates the remaining unknown parameters from the equivalent circuit

of the PICC via the passing parameters. The detailed calculation process is explained in section 6.2.7.

6.3.9 Function EMVCo Vpp

Passing parameters:

- Vector states of current \underline{I}_2
- Voltage states of calibration coil U_d

Return parameters:

- Magnitude and angle of load modulation voltage Vpp
- Transformed transponder impedance Z'_T
- PCD antenna current I_1

Description:

This function estimates the EMVCo parameter V_{pp} (load modulation voltage) through the measured values of the PCD and the PICC impedance. The measured values for EMVCo PCD are explained and shown in section 5.2. Generally, the effect of load modulation to the reader current can be similarly calculated with formulas 4.3.2 to 4.3.6. As the PICC has a different loading effect to the PCD than the calibration coil, the measured field strength values in table 5.4 are not exactly correct for the calculation. Therefore, an iterative algorithm is needed to calculate the correct field strength for the PICC. The loading effect is calculated for every iteration with the given PICC parameters. Basically, the loading effect decreases the field strength because the transformed transponder impedance decreases the PCD current (illustrated in figure 4.9). The next iteration calculates the real field strength and updates the PICC parameters. This iterative algorithm is done until the parameters converge.

Chapter 7: Conclusion

RFID applications are very common and the product portfolio is rising continuously. As a result, the data rate for the communication between reader and transponder has to increase too, because more information needs to be exchanged. The faster communication rates of the RFID system have to work correctly for the defined operating range. This master's thesis especially concentrates on the modulation of a contactless proximity chip card. As the product portfolio of the appropriated readers is huge too, several standardizations describe the requirements for chip cards.

The aim of this master's thesis was the development of an extended analysis tool for load modulation related to the existing measurement standards.

First of all, a general literature research was done for a better understanding of RFID systems. Furthermore, the analysis of load modulation according to the standards and regulations of ISO and EMVCo were investigated. Additionally, a simulation tool was used for the generation of an equivalent circuit of the RFID system and for analysis. An existing tool from Infineon was modified for data acquisition via the ISO set-up. Afterwards, the basic analysis according to the ISO standard was implemented in a Matlab script, which measures the level of the sidebands from the modulated transponder current. During this process, measurement problems occurred and were solved afterwards. On the one hand, a software bug concerning the data storage of the oscilloscope was solved, and on the other hand the specifics of the ISO tower measurement bridge were investigated. It was also established, that the oscilloscope probes have an enormous influence on signal acquisition. Firstly, the probes have an impact on the phase part of the bridge signal and secondly it is important to use probes of the same type, because otherwise run time delays would be different. Since the correct signal acquisition and data storage was established, the Matlab script was extended for further detailed investigations. Furthermore, a GUI was created for the interaction with the user. The next point was the analysis of the common Infineon chips and their comparison among themselves. For reasons of company secrecy, the obtained outcomes could not be written into this master's thesis. However,

the Matlab analysis tool could show general new insights related to the Infineon chips. The multiple analysis option of the Matlab script generated significant figures for chip comparison. By means of that results, a feedback to the chip designer could be given. In the same way, the implementation of the analysis option for the EMVCo set-up was done. During the master's thesis the idea came up, how the relation between the two standard test set-up's could be formed to one. As the ISO set-up is an automatic measurement system compared to the EMVCo set-up, it was taken for data acquisition and the values for EMVCo standard were calculated mathematically. It was noted, that the ISO set-up can be used for the parameter finding of the chip and the resonance frequency of the PICC. Otherwise, these parameters have to be measured manually with an impedance and network analyzer. As this process is very time-consuming and the measurement devices are very expensive, this concept is very promising and will be investigated in more detail in the future. It is important to say, that the measurement of the resonance frequency via the ISO set-up is a great opportunity, because many business partners and customers of Infineon could use it, especially those who don't have expensive measurement devices. The evaluation of the chip parameters can save a lot of time because the measurement via the ISO set-up can be adapted by an additional circuit board, which enables the automatic measurement of more than one chip during one pass. In the near future, the Matlab tool will be integrated in the internal measurement tool of Infineon, which is programmed in LabVIEW.

In summary, this master's thesis has generated an analysis tool for load modulation that will be used in the future and it has discovered important facts about the standard measurement set-ups.

Bibliography

- [1] ATIS Committee PRQC: ATIS Telecom Glossary 2011. Techn. Rep., 2011. <http://www.atis.org/glossary/images/wavefrmc.gif>.
- [2] Austrian Institute of Technology: Test PCD Assembly. Techn. Rep., 2009. http://www.ait.ac.at/fileadmin/mc/mobility/downloads/Test_PCD_assembly.pdf.
- [3] Bartsch, H.-J.: Taschenbuch Mathematischer Formeln. Carl Hanser Verlag, 2007.
- [4] Dunlop, J. and D. Smith: Telecommunications Engineering, Third Edition. Chapman and Hall, 1994.
- [5] Finkenzeller, K.: RFID Handbook - Second Edition. Carl Hanser Verlag, 2003.
- [6] Gebhart, M.: Vorlesung RFID Systems. online, 2009. <http://www.iks.tugraz.at/lehre/unterlagen/rfid-systems/1-einleitung>.
- [7] ISO/IEC: ISO/IEC 14443, Proximity cards. Techn. Rep. Part 2: Radio frequency power and signal interface, Committee identification: ISO/IEC JTC1/SC17/WG8, 2010-09-01. Identification cards: Contactless integrated circuit(s) cards - Proximity cards.
- [8] ISO/IEC: ISO/IEC 10373, Identification cards - Test methods. Techn. Rep. Part 6: Proximity cards, Committee identification: ISO/IEC JTC1/SC17/WG8, 2010-12-15. Identification cards: Contactless integrated circuit(s) cards - Proximity cards.
- [9] Kuchling, H.: Taschenbuch der Physik. Verlag Hari Deutsch, 1995.
- [10] MasterCard: Paypass- ISO/IEC 14443 Implementation Specification. Techn. Rep. Version 1.1, MasterCard International Incorporated, 2006-03-31. Identification cards: Contactless integrated circuit(s) cards - Proximity cards.
- [11] Rampetzreiter, S.: Very High Bit Rate Communication Channel Modeling on Inductively Coupled, Passive RFID Systems. Master's Thesis, 2009.

- [12] Rankl, W. and W. Effing: Handbuch der Chipkarten - 5 Auflage. Carl Hanser Verlag, 2008.